國立交通大學

光電工程研究所

碩 士 論 文

二維非均勻極化光之合成

2D Synthesis of Spatially Inhomogeneous
Polarized Beam

研 究 生：潘紀豪

指導教授：田仲豪　助理教授

中 華 民 國 九 十 七 年 七 月

二維非均勻極化光之合成

2D Synthesis of Spatially Inhomogeneous Polarized Beam

研 究 生：潘紀豪　　　　　Student：Chi-Hao Pan

指導教授：田仲豪　　　　　Advisor：Dr. Chung-Hao Tien

國立交通大學

光電工程研究所

碩士論文

A Thesis

2D Synthesis of Spatially Inhomogeneous Polarized Beam

National Chiao-Tung University

in Partial Fulfillment of the Requirements

for the Degree of Master

in

Electro-Optical Engineering

July 2008

Hsinchu, Taiwan, Republic of China

中華民國九十七年七月

二維非均勻極化光之合成

碩士研究生：潘紀豪　　　導教授：田仲豪 助理教授

國立交通大學

光電工程研究所

摘要

　　非均勻極化光近年來因其焦平面特別的強度分佈特性，所以被廣泛的研究討論，可運用於微粒補捉、材料處理、高解析度光學顯微鏡等領域。其中最知名的非均勻極化光為軸向對稱光，包含了徑向對稱極化光和角方向對稱光，這二兩種光都有這甜甜圈形狀的強度分佈，而不同的對稱極化分佈則可以在焦平面上得到不同的場分佈，例如徑向對稱極化光則可以得到較小的光點。具備達到或超越向量繞射限制的技術和在焦平面場分佈設計成為我們研究和發展的重心。藉由圓極化和相位調變器，可以將軸向對稱光拓展成為空間非均勻的任意極化光場。

　　基於以上論述，在此論文中，我們的目標是建立一光學系統來合成空間上非均勻極化光，這使我們可以在空間上方便的設計不同的極化分佈。為了可以動態的即時控制，我們採用干涉式的架構來合成均勻極化光。合成系統的穩定性將藉由我們校正技術來調整，而這個技術主要是利用系統中光渦的干涉圖像。最後這個方法的可行性，將由實驗的結果得到驗證。

2D Synthesis of Spatially Inhomogeneous Polarized Beam

Master student：Chi-Hao Pan   **Advisor**：Dr. Chung-Hao Tien

Department of Photonics ＆ Institute of Electro-Optical Engineering

National Chiao Tung University

ABSTRACT

Recently inhomogeneous polarized beams have been widely noticed due to their novel focal behavior for optical trapping, material analysis, and high-resolution imaging. The most well-known inhomogeneous polarizations include radial and azimuthal symmetry associated with donut-shaped pupil irradiance. The idea of extending cylindrical vector beams to arbitrary inhomogeneous polarized beams was presented by using the circular polarization with phase modulation method. This study was aimed at reaching vectorial diffraction limit and focus spot shaping.

In the thesis, a home-built optical configuration to synthesize the spatially inhomogeneous polarized beams was demonstrated. The infereometric scheme based on dynamic phase control was adopted to synthesize the spatially inhomogeneous polarizaed beam in a effective and simple way. Moreover, the characteristics of the sharp focus was analysed by a unique eight-zone segmentation of polarization states, which can be further applicable for the optical encryption. In addition, the stability as well as phase calibration of synthesis was also discussed.

致謝

　　我首先要感謝我的指導教授　田仲豪老師在這兩年來對於外語表達能力及研究上細心及嚴屬的指導，並在生活上提供良好的研究環境以及傳授許多人生的經驗，不僅幫助我順利完成此論文，也獲得許多寶貴的經驗及建議。

　　還必須感謝子翔學長在各方面對我的指導及協助，讓我在實驗思維上以及做事方式上有很大的新的體驗，也讓我有機會聽到這世界上一些新的概念。除此之外，壁如學姊在我初進實驗室時，人生地不熟時的寶貴意見也給予我很大的幫助。也感謝洪健翔、陸彥行，簡銘進等其他實驗室的學長們給予珍貴的意見及生活上的協助，尤其是翔翔時而搞笑時而認真的態度，不愧是本實驗室的委員長。同時感謝洪瑋琮、呂柏毅、蕭人彰、鍾積賢、余宗翰等同學們在研究、生活、音樂上的幫助和專業咨詢。也感謝實驗室學弟妹，張永昇、林鳳玲、林宗瑋、董雨朧，讓實驗室充滿新清健康的氣氛。

　　最後我要感謝我的家人，感謝你們從小的栽培及照顧，讓我無後顧之憂的專心於研究，也感謝你們放任我想做什麼就做什麼，讓我可以慢慢的找尋自己人生的方向。最後將這分喜悅分享給每一個關心我的人。

Table of Contents

Figure Captions

List of Tables

Chapter 1

Introduction

Introduction

Optics is always one of the most exciting regions in physics. For centuries conducted in parallel to the discovery of nature of light, the investigations including the manipulation and focusing of light soon hit one of the fundamental limits. The resolution of image quality was limited by the nature of light depended on the wavelength and the numerical aperture (NA) of the lens.

The mathematical theory correlating resolution to the wavelength of light was formulated by Ernst Karl Abbe (1840–1905). For most optical systems the resolution is limited by approximately a half wavelength of the illumination light. Recently, a branch of ideas and mechanisms was proposed to overcome the scalar diffraction limit. This rising interest in polarization based research is investigated in a time where crucial technological areas are approaching fundamental limits. For sharply focusing the beam in large number of optical instruments, the polarization properties of electromagnetic field play a dominant role. The Germany group showed that the size of focus spot is further reduced when applying the inhomogeneous polarized beams [1]. In this thesis, we focus on the synthesis system for generating the spatially inhomogeneous polarized beams.

1.1 Gaussian beams

In optics, a Gaussian beam is electromagnetic radiation whose transverse electric field and irradiance distributions are described by Gaussian functions. It is a simple way for us to adopt Gaussian beam as the light source when investigating some

1

physical effect. Gaussian beams can easily be extracted from some lasers setup which is said to be operating on the fundamental transverse mode (TEM$_{00}$ mode) inside laser resonated cavity. It is a peculiar transformation property that a Gaussian beam is transformed into another Gaussian beam when refracted by a lens. The mathematical function that describes the Gaussian beam is a solution to the paraxial form of the Helmholtz equation. The paraxial form of the Helmholtz equation is showed as

$$\left(\frac{\partial^2}{\partial x^2} + \frac{\partial^2}{\partial y^2}\right) A - j2k \frac{\partial}{\partial z} A = 0 \tag{1-1}$$

where $A(r)$ is a complex envelope and complex amplitudeis is $U(r, z) = A(r)\exp(-jkz)$. The solution $U(r, z)$, in the form of a Gaussian function, represents the complex amplitude of the electric field, which propagates along z axis with the corresponding magnetic field. For a Gaussian beam, the complex electric field is described as

$$U(r, z) = A_0 \frac{W_0}{W(z)} \exp\left(-\frac{\rho^2}{W^2(z)}\right) \exp\left[-jkz - jk\frac{\rho^2}{2R(z)} + j\zeta(z)\right] \tag{1-2}$$

where r is the radial distance from the center axis of the beam, z is the axial distance from the beam waist, k is the wave number, $W(z)$ is the radius where the field amplitude and intensity drop to $\frac{1}{e}$ and $\frac{1}{e^2}$ of their axial values, respectively. $w_0 = w(0)$ is the waist size (described in more detail below). The functions $R(z)$ is the radius of curvature of the wavefronts comprising the beam, which gives $R(z) = z[1 + \left(\frac{z_0}{z}\right)^2]$.

These are natural extensions of the fundamental lowest-order Gaussian solution. For real observation, the time-averaged intensity distribution is

$$I(r, z) = I_0 \left[\frac{W_0}{W(z)}\right] \exp\left(-\frac{2\rho^2}{W^2(z)}\right). \tag{1-3}$$

At each value of z the intensity is a Gaussian function of the radial distance r. For flat top light source required, one can expend the foundamental gaussian beam

with appropriate objective lens and collimator. Moreover, a suitable diaphragm is needed to put behind this beam expend to extract the smooth intensity distribution. In order to get a clean expanded Gaussian beam, it is necessary to use the spatially filter to remove aberrations in the beam due to imperfect, dirty, or damaged optics, or due to variations in the laser gain medium itself. Both the beam from the laser and the expanded beam will have a Gaussian intensity profile. After the collimated beam is expanded, we can extract the center part of the beam which is approximate exhibit smooth intensity distribution.

However, the Gaussian beam is not the only one solution for the paraxial Helmholtz equation. There are some interesting solutions of intensity distribution which can be satisfied with the conditions. When using cardisian coordinates, Hermite-Gaussian beam is another group of eigen modes for the paraxial Helmholtz equation. Moreover, in cylindrical coordinates it's convenient to use Laguerre-Gaussian polynominal for the eigen mode.

1.1.1 Hermite-Gaussian (HG) beams

Most laser cavities are associated with the retangualr symmetry. In transverse dimension the transverse field distribtuion of the laser beam is best described in term of Hermite-gaussian modes along the propagation axis. The optical intensity of Hermite-Gaussian beam is

$$I_{n,m}(x,y,z) = \left|A_{(n,m)}\right|^2 \left(\frac{w_0}{w(z)}\right)^2 G_n^2\left(\frac{\sqrt{2}x}{w(z)}\right)G_m^2\left(\frac{\sqrt{2}y}{w(z)}\right) \tag{1-4}$$

where the function $G_n(x)$ is the Hermite function of order n, and $A_{n,m}$ is a constant [2]. For the case $(n,m) = (0,0)$, the equation describes a Gaussian beam which is the only cirularily symmetric member of HG beams. Gaussian Intensity distribution of several

Hermite-Gaussian beams in the transverse plane is illustrated in Fig. 1-1.

(a) (0,0)   (b) (0,1)   (c) (0,2)

(d) (1,0)   (e) (1,1)   (f) (1,2)
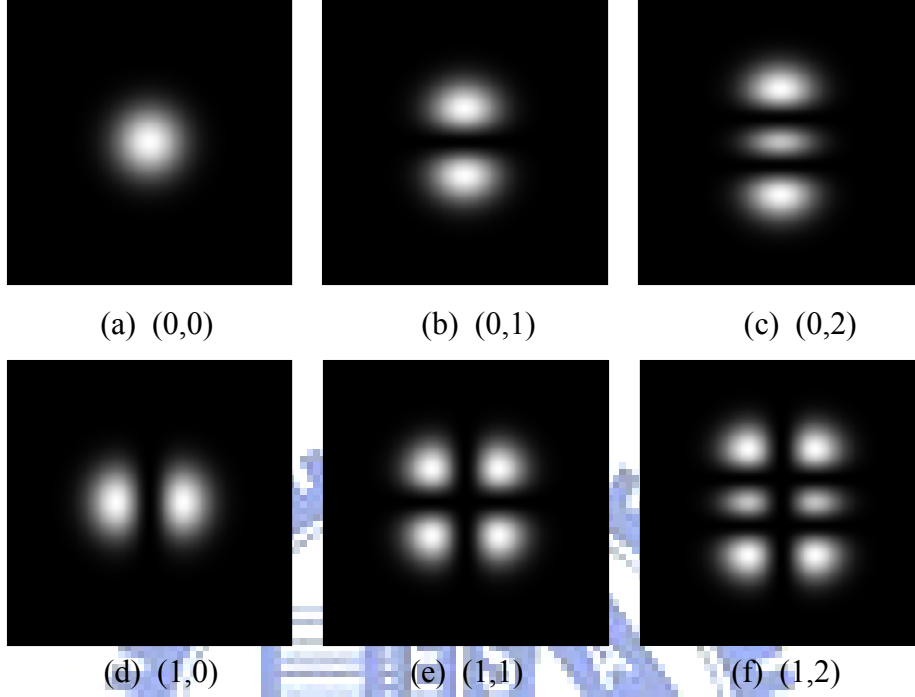
Fig. 1-1. Intensity distribution of several Hermite-Gaussian beams in the transverse plane. The order (m, n) is indicated in each case.

1.1.2 Laguerre-Gaussian(LG) beams

If we consider the laser cavity in cylindrical coordinates, higher order modes form a complete basis set by using Laguerre- instead of Hermite-polynomials. In this manner the field of two dimensional Laguerre-Gaussian modes may be written as

$$u(r, \phi, z) = \frac{C_{mp}^{LG}}{w(z)} (\frac{\sqrt{2}r}{w(z)})^m L_p^m \left(\frac{r^2}{w(z)^2}\right) \exp\left(-ik \frac{r^2 z}{2(z^2 + z_R^2)}\right)$$

$$\times \exp\left(i(2p + m + 1)\tan^{-1}\left(\frac{z}{z_R}\right) - im\phi\right) \qquad (1\text{-}5)$$

where C_{mp}^{LG} is the normalization constant, and L_p^m are the generalised Laguerre polynomials [3]. The index m is the azimuthal index and refers to the number of complete (2π) phase cycles around the circumference of the mode. The radial index

$p \geq 0$ and (p + 1) gives the number of radial nodes in the mode profile..

Differently from Hermite-Gaussian beams, Laguerre-Gaussian modes have rotational symmetry along their propagation axis and carry an intrinsic rotational orbital angular momentum of $i\hbar$ per photon [4][5]. This means that a refractive object placed along the propagation axis will experience a torque. This property of LG beams is of considerable practical interest, particularly in the field of optical trapping and for driving micromachined elements with light. It may be noted that this intrinsic rotational momentum has to be distinguished from the angular momentum due to the polarization of light. Fig. 1-5 shows the intensity distribution of various LG modes in the transverse plane. We can find that the dark core is larger as the index m is increasing. This is because the more helical phase of azimuthal index include the more numbers of complete (2π) phase cycles. Phase distribution of several LG beams is described in Fig. 1-3. Such spiral phase lead to the optical vortex which will be introduced in the Chapter 3.

(a) (0,0)   (b) (0,1)   (c) (0,2)

(d) (1,0)   (e) (1,1)   (f) (1,2)
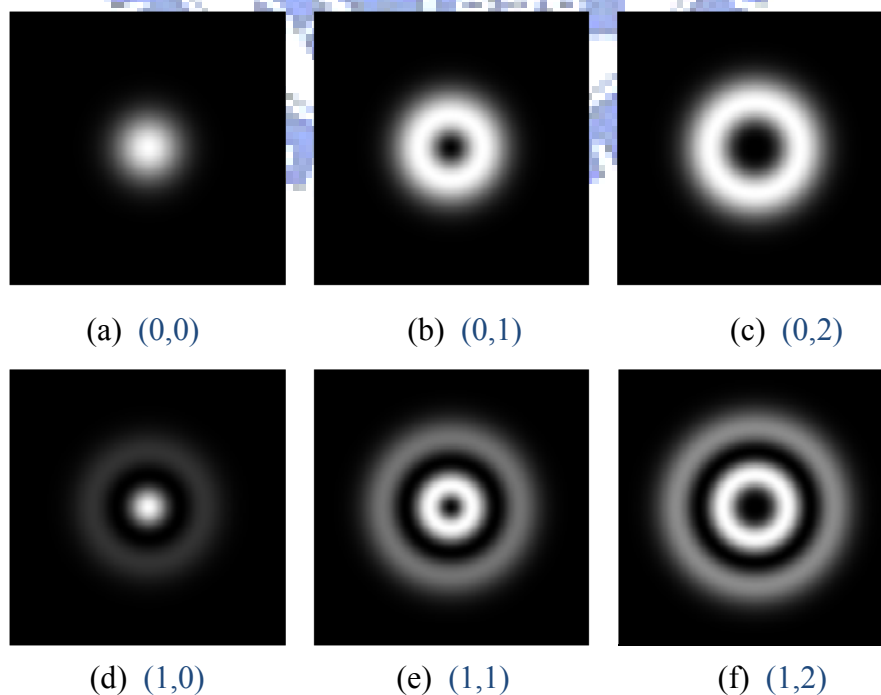
Fig. 1-2 Intensity distribution of different Laguerre-Gaussian beams in the transverse

plane. The order (p, m) is indicated in each case.

<center>(a)   (b)   (c)</center>

<center>(d)   (e)   (f)</center>
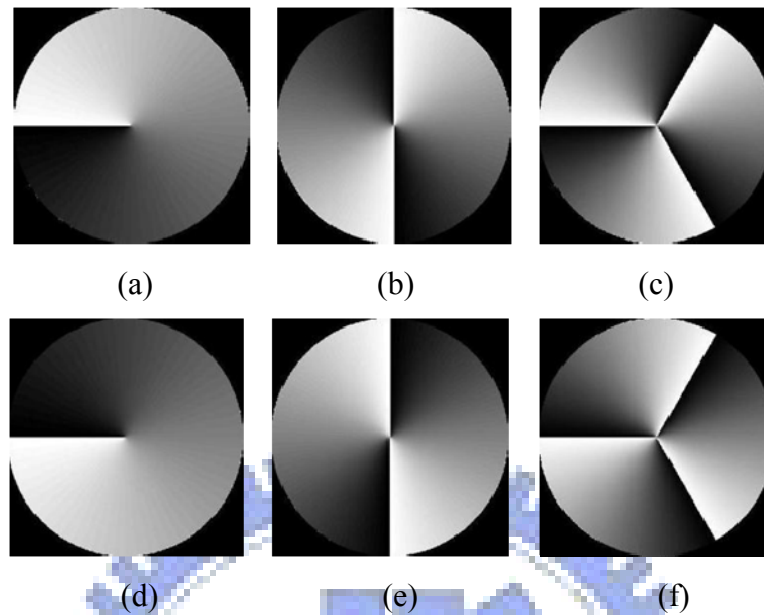
Fig. 1-3 Phase distribution of different Laguerre-Gaussian beams in the transverse plane. The index m is (a)1, (b)2, (c)3, (d)-1, (e)-2, (f)-3.

No matter what the HG and LG modes each form complete basis sets, any arbitrary field distribution can be described by an appropriate superposition of these eigen modes. Any LG mode can be expressed in terms of HG modes and vice versa [2]. According to this property the beam could be synthesized by using HG or LG beams and the following content will be introduced recently to explore the formation of the inhomogeneous beam in coherent systems.

1.2 Spatially inhomogeneous polarized beam

The beam with the same polarization at every point within the pupil plane is homogenous polarization, i.e. $\vec{E}(x,y) = Ex\hat{x} + Ey\hat{y}$. We can describe the field distribution by using the function depending on the ratio of Ex and Ey. If the beam only have the Ex component, it is the linear x-polarized beam which can be generated by passing the incident beam through a polarizer. If the phase delay between Ex and

<center>6</center>

Ey is 90°, the beam become the circular polarization. Fig. 1-4(a) is the illustration of homogenous beams which are x-polarization, right hand and left hand circular polarization, respectively.

On the other hand, the spatially inhomogeneous beam has particular state of polarization at every local point of pupil plane, as shown in Fig. 1-4(b). The local field gives the following function: $\vec{E}_{li}(x_{li}, y_{li}) = Ex_{li}\hat{x} + Ey_{li}\hat{y}$ where li means the i index of local point. The total field in pupil plane can be summated by each state of polarization and the field shown as

$$\vec{E}_{total}(x, y) = \sum_{i=1}^{n} \vec{E}_{li}(x_{li}, y_{li}).$$ (1-6)
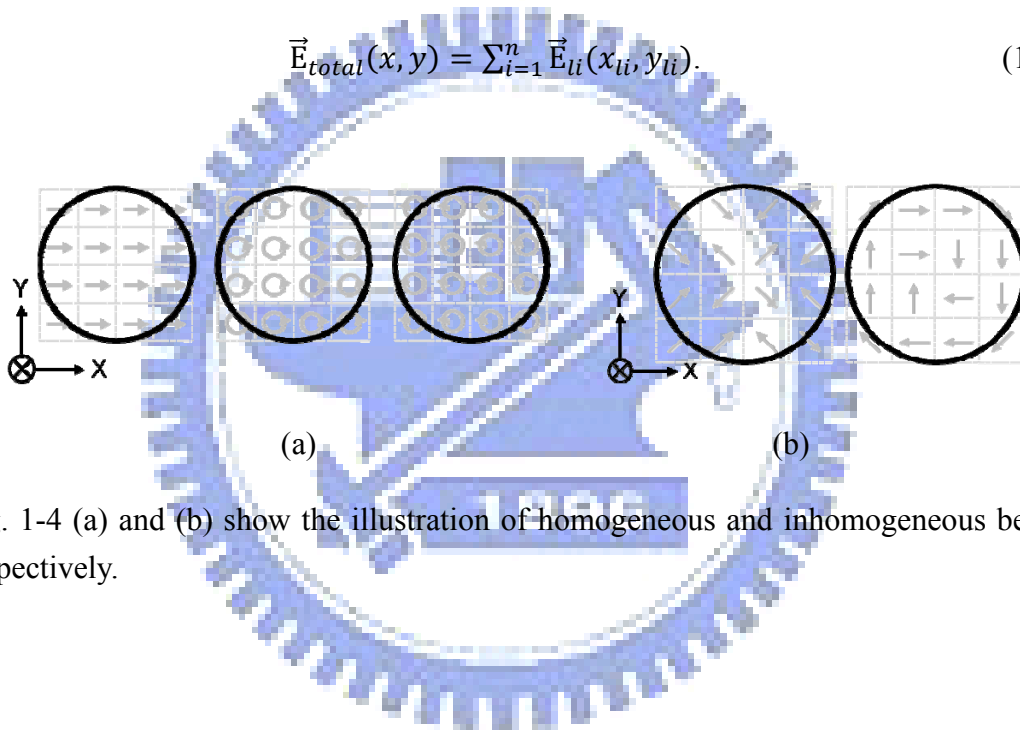
Fig. 1-4 (a) and (b) show the illustration of homogeneous and inhomogeneous beam respectively.

1.2.1 Cylindrical vector beams

Cylindrical vector beams with good symmetry on polarization is one kind of the spatially inhomogeneous beams[14]. Since cylindrical vector beams have attracted much attention in recent years due to their unique properties caused from the polarization [13][14]. The general solution of the wave equation for cylindrical vector beams consists of two independent solutions: azimuthally polarized beam and radially polarized beam. Such solutions which obey cylindrical symmetry not only in

field-amplitude but also in polarization have been the topic of numerous recent theoretical and experimental investigations. The orthogonal cylindrical vector beams have the donutlike irradiance and good symmetry in r-direction or ϕ-dircection, as showed in Fig. 1-5. The formula of radially and azimuthally polarized beam can be simply described by $\vec{E}_{RP}(r,\phi) = E_0(r)\hat{r}$ and $\vec{E}_{AP}(r,\phi) = E_0(\phi)\hat{\phi}$, respectively.

(a)　　　　　　　　　　　　　　(b)
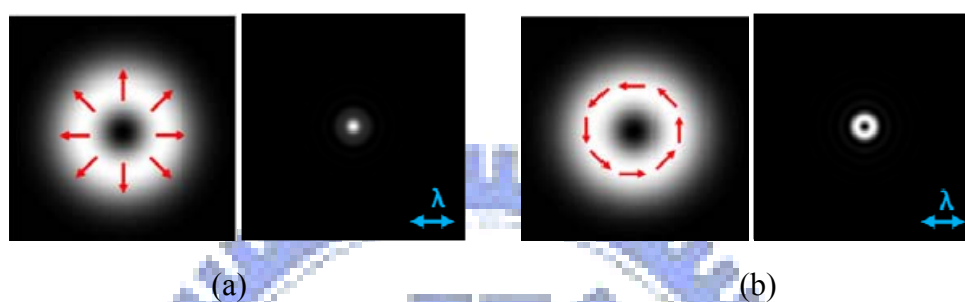
Fig. 1-5 The intensity distributions of the cylindrical vector beams and their focal spot. (a) Radially polarized beams and (b) azimuthally polarized beams. The arrows represent the polarization directions.

In spite of identical donut-shaped pupil irradiance and axially symmetrical polarization, the longitudinal electric component of the focus between radial and azimuthal beams exhibits a huge discrepancy. Due to the strong depolarization effect in high numerical aperture (NA), radial direction of polarization can generate a high longitudinal component at focus, therefore, which results in an ultrasmall focal spot. In the other words, cylindrical vector beams with radial polarization could be focused tighter than diffracted limited spot [1]. However the property could further improve the resolution of the point spread function and could be applied such as particle-trapping [16], particle acceleration [17], optical data storage and micro-lithography [18]. In contrast, the azimuthal polarization created an optical cage with the absence of electric longitudinal component at the vicinity of focal point.

A recent project that we have been working on involves polarization and the

geometric phase that results from cyclic changes in the cylindrical vector beams. Cylindrical vector beams can be generated by various methods and some of them are associated with Gaussian beam.

1.3 Motivation and Objective

Taking aforementiond concerns into account, it has been demonstrated in some applications that inhomogeneous beams are needed for many application. In light of these concerns, three main demands to drive us to investigate inhomogeneous polarized beam: (a) to reach vector diffraction limit; (b) focus spot shaping; (c) polarization carried optical information. Due to the better syncronization in dynamic control we present a method to synthesize the spatially inhomogeneous beam. The method of synthesis is infereometric setup with spatial light modulator. A interference pattern was observed in the exit puiple plane because of the tilted angle of the optical path. The stability of expreimental setup was discussed through analysis of the optical vortex phase. The pracicality of the proposed methodology is demonstrated through experimental result.

This thesis covers three main topics: (1) The synthesis of a cylindrical vector beams and (2) the properties of a partially coherent vortex field and (3) the synthesis of 2D synthesis of inhomogeneous polarized beam. Therefore, it is aimed to set up the optical system to synthesize the spatially inhomogeneous polarized beams.

1.4 Organization

The performance of synthesis of the inhomogeneous beams will be theoretically predicted and experimentally verified. First the relevant physical and

optical aspects, such as Gaussian beam are described. In order to let laser beam field carry with the desired optical properties, in chapter 2 the theory of the formation of cylindrical vector beams is described. Also the fabrication process of the experimental setup will be introduced.

In Chapter 3, the optical vortex will be discussed due to its spiral phase which caused interesting interference pattern. An initial experimental verification of the theoretical predictions is performed by measuring irradiance of exit of interferometer.

Furthermore, we demonstrated a method to synthesis the specific directions of polarization based on our synthesis setup in Chapter 4. Also a theoretical framework is developed to describe the inhomogeneous polarization. Finally, the conclusions and the future works will be described in Chapter 5.
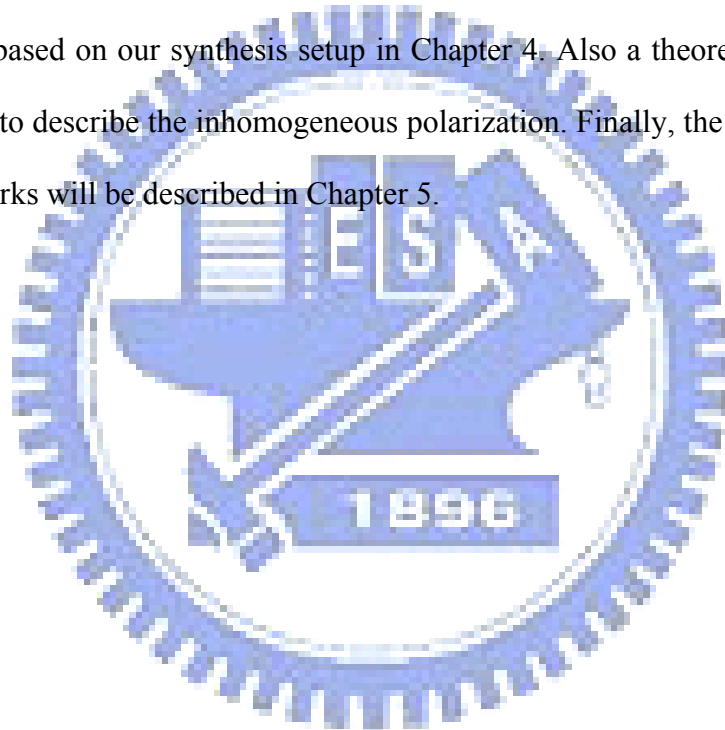
Chapter 2

Principle and setup

Interferometric method was proposed to synthesize the inhomogeneous beams. In this chapter, I will introduce the main principle of synthesis process of cylindrical vector beams. The experimental setup and the limit of instrument will be introduced in the following.

2.1 Synthesis of cylindrical vector beams

The polarization of cylindrical vector beams is highly symmetric. Different methods have been adopted to synthesize cylindrical vector beams, and the synthesis process can be distinguished into the two catalogs: inside or outside cavity. Outside the resonator cylindrical vector beams are obtained by transmitting linear polarized beams through a twisted nematic liquid crystal [10], spatially variable retardation plate [7], or subwavelength grating [9]. Another technique was demonstrated by inserting a phase element into a laser resonator for selecting specific modes and the phase element could be mode converter, bisect phase retardation [12], and polarization selective mirrors [6].

In this thesis, the synthesis was achieved by use of the interference method with the phase modulator [10][11]. Because the pattern of the phase modulator is easily operated and changed, interference method achieves better synchronization in the dynamic control. Moreover, interferometric synthesis of the cylindrical vector beams can be basically distinguished to two approaches: one is linear polarization approach and the other is circular polarization approach.

2.1.1 Linear polarization approach

Any cylindrical vector beams can be decomposed into two eigenmodes. The directions of polarization of each eigenmode are mutually orthogonal and can be expressed in Cartesian or polar coordinates. In Cartesian coordinates two orthogonal Hermite-Gaussian modes TEM_{10} and TEM_{01} with specific linear polarization can be used to synthesize cylindrical vector beams. The intensity of HG without polarization can be described by the following formulas:

$$\vec{E}_1(r,\phi) = E_0(r)\cos(\phi) \tag{1}$$

$$\vec{E}_2(r,\phi) = E_0(r)\sin(\phi) \tag{2}$$

where r is the radial distance from the origin, and ϕ is azimuthal angle in cylindrical coordinates. E_0 is the amplitude of the electric field. The linear combination of TEM_{10} with x-polarized beam and TEM_{01} with y-polarized beam can be achieved by using Mach-Zehnder interferometer. In mathematics the simple addition can yields

$$\vec{E}_{RP}(r,\phi) = E_1\hat{x} + E_2\hat{y} = E_0[\sin(\phi) + cos(\phi)\hat{y}] = E_0(r)\hat{r}. \tag{3}$$

Where the symbol $\hat{x}$ and $\hat{y}$ are the unit vectors of Cartesian coordinates. Similarly, the coherent summation of TEM_{10} with y-polarized beam and TEM_{01} with x-polarized beam leads to the formation of azimuthally polarized beams. In mathematics the simple addition can yields

$$\vec{E}_{AP}(r,\phi) = \vec{E}_1\hat{y} + \vec{E}_2\hat{x} = E_0[\cos(\phi)\,\hat{x} - sin(\phi)\hat{y}] = E_0(\phi)\hat{\phi}. \tag{4}$$

At the exit pupil of interferometer, the radially polarized beam can be observed. Fig. 2-1 illustrates the synthesis process.
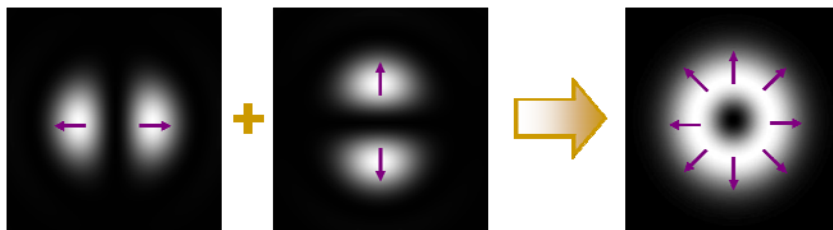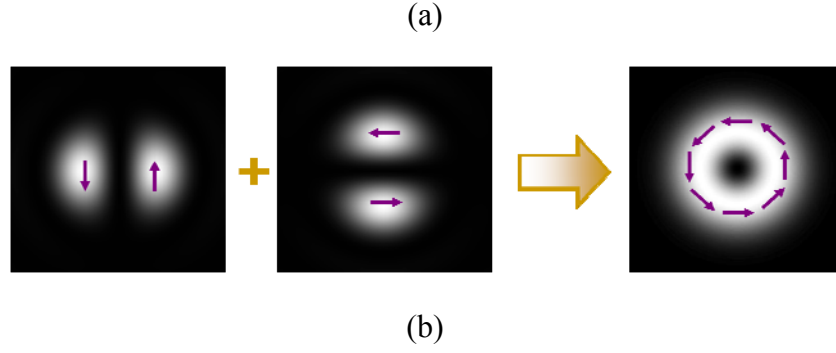
Fig. 2-1 Synthesis process of cylindrical vector beams by combining linearly polarized HG_{10} and HG_{01} mode. (a) Radial polarization of combining HG_{10} with x-polarization and HG_{01} with y- polarization. (b) Azimuthal polarization of combining HG_{10} with y-polarization and HG_{01} with linear x- polarization.

The local polarization of cylindrical vector beams is generated by combining two states of polarization with different intensity distribution. When using the linear approach, we can find that intensity is a big issue. The intensity distribution of HG beams shall be produced so the intensity modulator is needed. However, the pure intensity modulator is not easily collimated and changed but it is straightforward to understand the synthesis process.

2.1.2 Circular approach

Another method of interfereomatrically synthesize the cylindrical vector beams is using circular approach. We adopted numerical manipulation to analyze the summation of two orthogonal fields with opposite-handed circularly polarized Laguerre-Gaussian beams, which are presented as below.

$$\vec{E}_1(r, \phi) = \frac{1}{2} E_0(r)(\hat{x} - i\hat{y}) \exp(i\phi) \tag{1}$$

$$\vec{E}_2(r, \phi) = \frac{1}{2} E_0(r)(\hat{x} + i\hat{y}) \exp(i\phi) \tag{2}$$

Eq. (1) and (2) describe two opposite circular wave through the spiral phase. By

superposing $\vec{E}_1$ and $\vec{E}_2$, radial polarization can be obtained and expressed as Eq. (3).

$$\vec{E}_{RP}(r,\phi) = \vec{E}_1 + \vec{E}_2 = E_0[\sin(\phi)\,\hat{x} + i\cos(\phi)\hat{y}] = E_0(r) \tag{3}$$

Similarly, azimuthal polarization is obtained by adding 90°phase delay into Eq. (2) and the summed form was shown in Eq. (4).

$$\vec{E}_{AP}(r,\phi) = \vec{E}_1 + \vec{E}_2 e^{i\pi} = E_0[\cos(\phi)\,\hat{x} - i\sin(\phi)\hat{y}] = E_0(\phi) \tag{4}$$

Fig. 2-2 illustrates the synthesis process.
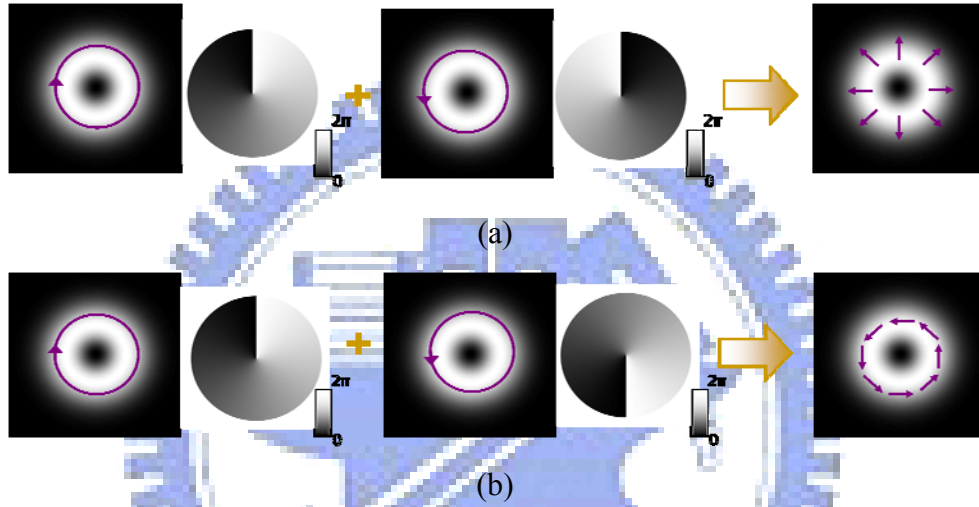
Fig. 2-2 Synthesis process of cylindrical vector beams by combining circularly polarized LG_{01} and LG_{0-1} mode. (a) Radial polarization of combining LG_{01} with left-handed circularly polarization and LG_{0-1} with right-handed circularly polarization. (b) Azimuthal polarization of combining LG_{01} with right-handed circular polarization and LG_{0-1} with left-handed circular polarization. Each sub-picture includes the intensity distribution on the left and the phase distribution on the right.

For circular polarization approach the local polarization of cylindrical vector beams is generated by combining two states of polarization with different phase distribution. When using the circular approach, we can find that phase is a big issue. The phase distribution of LG beams could be easily produced by using Spatial Light Modulator (SLM) which will be discussed in next section. Because of the convenience of SLM, we adopt the circular approach to synthesize the cylindrical vector beams.

2.2 Experimental setup

The experimental configuration of polarization synthesis was schematically showed in Fig. 2-3. A $\lambda = 632nm$ laser beam is first collected and directed toward the spatial light modulator. SLM was halved and modulated with the corresponding phase arrangement. After reflected by the SLM, two coherent beams are transformed into flat top Laguerre-Gaussian beam associated with different spatial phase distribution. Two beams are separated by using the appropriate diaphragm. Furthermore, the polarizer with a quarter wave plate converts the linearly LG beams to right/left handed circularly polarized beams in each arm of the optical path. The interference between individual optical beams leads to the radially or azimuthally polarized beam, respectively. Finally, the pupil radiance is observed by a CCD at the exit pupil of lens. Moreover, we can use SNOM system to measure the near field of interaction between the incident synthesized beams and the test sample or observe the information of reflected beams by CCD, as depicted in Fig. 2-3(b). In the following the instruments such as SLM, interferometer and SNOM are discussed in detail.
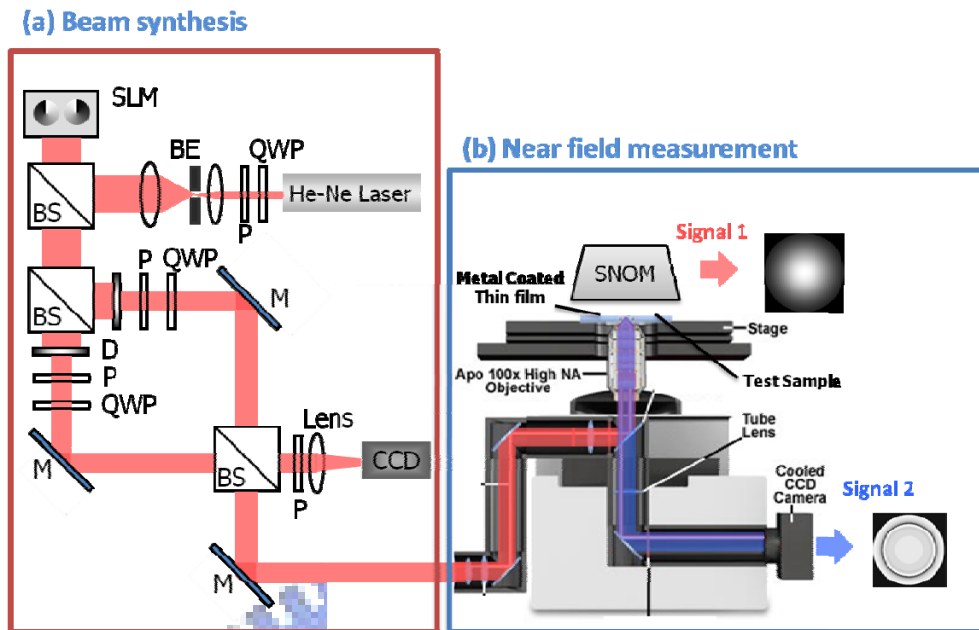
Fig. 2-3 The experimental setup. (a) Beam synthesis system. (b) Near field measurement.

2.2.1 Spatial Light Modulator (SLM)

A Spatial Light Modulator (SLM) usually modulates the intensity and the phase of beams simultaneously or individually. The SLM accepts the pattern information from the host computer and manipulate input coherent light source carried with designed phase information. Desirable modulation of intensity or phase in the visible makes this device to a good choice for plenty of applications such as projection, adaptive illumination, optical tweezing, active wave front control and reconstruction of coherent optical information processing sensing, etc.

SLM systems for phase modulation of coherent light sources are mainly MEMS- (Micro-Electro-Mechanical Systems) or LCD- (Liquid Crystal Display) based. Our choice of SLM is LC-R 2500 showed in Fig. 2-4 which is one of the reflective SLMs based on 2-dimensional arrays of LC cells (displays). The display can simply be

connected and driven by a personal computer and behave like a second monitor which

is based on a XGA (1024×768 pixel) back plane with a 19 μm pixel pitch.

Fig. 2-4 The spatial light modulator (SLM) LC-R 2500.

The operation of LC devices is based on the principle of birefringence. Birefringence is the phenomenon in which the phase velocity of an optical wave propagating in the crystal depends on the direction of its polarization. By applying a voltage to the LC device, its optic axis is aligned in a direction perpendicular to the electrode plates. A change in the polarity of the voltage results in rotation of the optic axis. By using a combination of the LC crystal, suitable polarizing optics and by switching the polarity of the applied voltage, it is possible to transmit or absorb an input light beam. The LC device can be used to perform both amplitude and phase modulation of the input light.

For LC-R 2500, the phase can be modulated more than 2π but amplitude also be modulated due to polarization rotation of the twist in the liquid crystal cell. Between a analyzer and a polarizer, the polarization rotation of SLM introduces an always present residual amplitude modulation which worse the performance because pure phase modulation is required for our experiment. The measurement of the instruction was done for a polarizer and analyzer setting which results in a low amplitude

modulation at 633nm, as showed in Fig. 2-5. Due to the deviation of intensity modulation it causes the bad uniformity and some aberration of the synthesized beams.

The lookup table (LUT) gives an output value for each of a range of index values such as the gray level. One common LUT is used to determine the colors and intensity values with which a particular image will be displayed. For our experiment, the output of phase retardance in units of degree is associated to the respective gray level form 0 to 256 in the LUT, as depicted in Fig. 2-6.
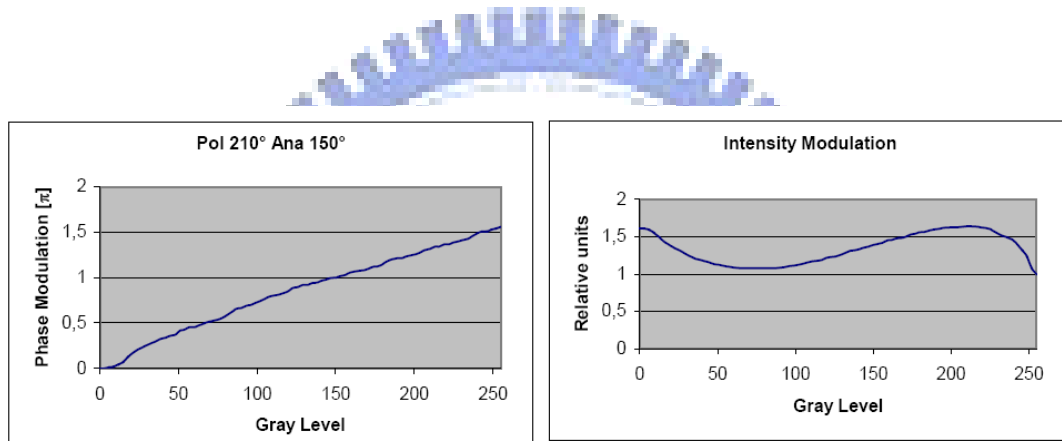
Fig. 2-5 Polarizer and analyzer setting for low amplitude modulation at 633nm in the instruction.
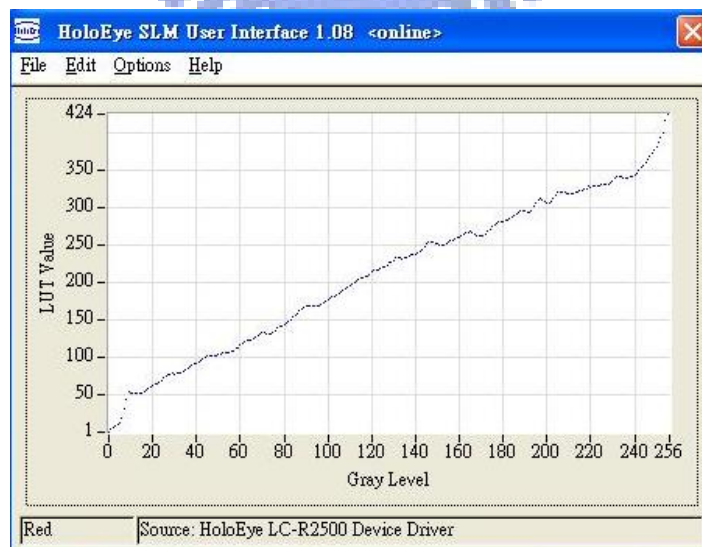
Fig. 2-6 The look-up table in the software driving the SLM for our experiment.

2.2.2 Interferometer

An interferometer is an optical device which utilizes the effect of superposition. Typically, it starts with input beam, splits it into two separate beams with some kind of beam splitter or a partially transmissive mirror. We can possibly expose some of these beams to some external influences such as some length changes or refractive index changes in a transparent medium, and recombines the beams on another beam splitter. The irradiance or the spatial shape of the resulting beam can be measured by some instruments such as CCD or the power meter.

The Mach-Zehnder interferometer was developed by physicists Ludwig Mach and Ludwig Zehnder. It is a device used to determine the phase shift caused by a transparent sample which is placed in the path of one of two collimated beams from a coherent light source. Moreover, it is a way to synthesize the beam caused by superposing two collimated beams with different arrangement.

As shown in Fig. 2-7, two separate beamsplitters (BS) are used to split and recombine the beams, and two outputs can sent to photo detectors or SNOM for the measurement. The optical path lengths in the two arms may be nearly identical, and each of two paths includes a polarizer and a quarter wave plate which lead to the circular polarization. The correct match between the phase pattern on SLM and polarization leads to the desired beam, and then the final irradiance of combination can be checked by simulation in chapter 2. If the interferometer is well aligned, optical path with no tilted angle make the resulting beams perfect. Besides for misaligned beams, i.e. with one mirror being slightly tilted, there will be some fringe patterns in both outputs, and variations of the tilted angle difference affect mainly the

shapes of these interference patterns.
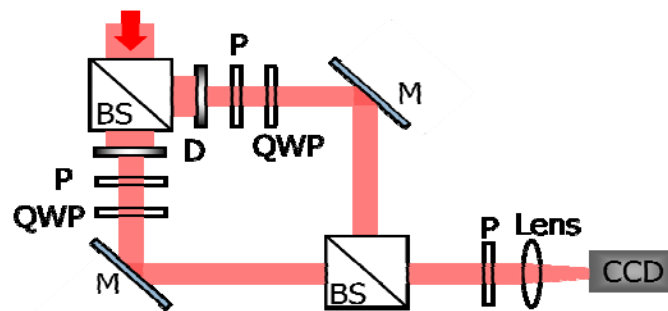
Fig. 2-7 The Mach-Zehnder interferometer. BS: beamsplitters, M: mirror, and
D: diaphragm.

2.2.3 Scanning Near-Field Optical Microscope (SNOM)

The SNOM is a specialized scanning probe microscope (SPM) measurement
system built on the platform. A SNOM measuring head lies in the basis of this system.
SNOM techniques are used to study near-surface optical characteristics (including
luminescent and spectral) of various objects with resolution much greater than the
diffraction limit. The higher resolution is gained by exposing samples with light going
through a diaphragm whose aperture is much less than the wavelength of the radiation
detected. The surface under study lies in the near field of the diaphragm (at distances
of about 10 nm).

The most advanced technologies used in the design of the system and the
powerful software make the SNOM easy to solve the following problems: (a) measure
surface topography of the sample under investigation, (b) measure surface optical
properties, and (c) Perform nano-lithography operations.

Our SNOM is called Solver SNOM which is designed and manufactured by
NT-MDT as showed in Fig. 2-8 (a). The Solver SNOM is based on the inverted

optical microscope Olympus IX81 as showed in Fig. 2-8 (b). For our purpose of measurement, the focal spot of our synthesized beam is obtained by Solver SNOM.

(a)   (b)
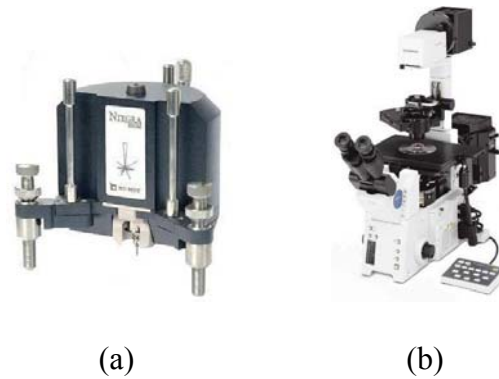
Fig. 2-8 (a) Solver SNOM. (b) Inverted optical microscope Olympus IX81.

2.3 Summery

Consideration of the better synchronization in the dynamic control, the circular approach of interference method was chose. Further, experiment setup was introduced. In the following chapter, we will use these instruments to accomplish the synthesis system, and the simulation software will be utilized to verify our system.

Chapter 3

Experiment and verification

The experiment of synthesizing the cylindrical vector beams and interference will be discussed in this chapter. First LG beam has the optical vortex phase which leads to wire patterns. The performance and the feasibility of our experiment setup would be obtained by checking these interference pattern .

3.1 Optical vortex

Optical vortices are characterized by a dark core of destructive interference in a coherent beam. The last decade has seen a resurgence of interest in optical vortices, owing to new potential applications. Optical vortices have been used to enhance laser trapping of low index particles, and laser tweezing of biological samples. In nonlinear optical systems, optical vortices may induce a waveguide, which may be useful as an optical switching technique. Optical vortices have also sparked interest in quantum computing due to their unique wavefront topology.

An optical vortex is essentially a helical phase and can be described by a phase profile given by:

$$\Phi(r, \phi, z) = m\phi \tag{3-1}$$

where (r, ϕ, z) are the cylindrical coordinates centered on the vortex, and m is a signed integer known as the topological charge or strength of optical vortex. The topological charge of a defect may be found from the line integral:

$$m = \left(\frac{1}{2\pi}\right) \oint \nabla \phi \, \mathrm{ds} \tag{3-2}$$

where $\nabla\phi$ is the gradient of the phase of the field and ds is a line enclosing the defect. Around the vortex center the helical phase increases by an integer multiple of 2π. Except the vortex centet(r=0) where the phase exhibits singularity, the phase distribution is continuous for all paths along ϕ direction. However, this singularity is physically acceptable due to the zeor intensity at the beam center.

A monochromatic light beam traveling along a given axis z can transport angular momentum oriented in two different forms. The first form is caused by circular polarization, and the photon carry $\pm\hbar$ of angular momentum depending on the handedness of the polarization. Another form is associated with optical phase distribution in the transversal plane. From the equation $\vec{E}(r,\theta) = E_0(r)\exp(im\theta)$, the photon propagate in the free space with the $m\hbar$ of angular momentum.

A single optical vortex in the center of a scalar monochromatic beam propagating in the z direction may be written in cylindrical coordinates (r, ϕ, z):

$$E(r,\phi,z,t) = E(r,z)e^{-im\phi}e^{ikz-iwt} \tag{3-3}$$

where E(r, z) is a circularly symmetric amplitude function, $k = 2\pi/\lambda$ is the wave number of a monochromatic field of wavelength λ, w is the angular frequency, and m is the topological charge. The amplitude and phase of a typical vortex beam are shown in Fig. 3.1. The vortex nature of the field is governed by the phase factor, e^{imf}. At a fixed instant of time helical surfaces of constant phase given by $mf - kz = const$ are produced for integer values of m. Along the helix axis $(r = 0)$ the phase is undefined and thus this point is known as a phase singularity. The amplitude also vanishes along the helix axis (r=0) owing to destructive interference in the vicinity of the vortex core i.e. $E(0,z) = 0$. The Laguerre-Gaussian modes are an orthonormal set of solutions to the wave equation in cylindrical coordinates and have the property of the optical vortices.
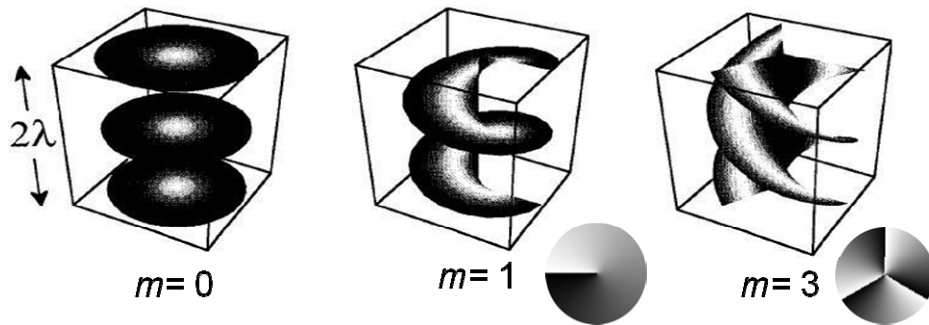
Fig. 3-1 Wavefront and phase distribution with different vortex beam number m.

3.2 Interference pattern

In general, when two or more scalar waves with the same polarization interfere in space, complete destructive and constructive interference occurs on lines called nodal lines, and on points called phase singularity, wave dislocation, or optical vortices. The standard Mach–Zehnder interferometer can merge two beams at the output of the interferometer. If one beam be tilted from the optical axis, irradiance of interference pattern can be obtained.

When using circular approach for the synthesis of cylindrical vector beams, the opposite topological charge was adopted in the interferometer. Consideration of tilting one beam leads to the interference pattern by passing through a polarizer. From difference of interference pattern, we can easily distinguish between the radially-polarized beams and azimuthally-polarized beams and check the precision of this synthesis.

3.2.1 Analytical description of interference

The adopted method of synthesizing the inhomogeneous beams is circular polarization approach, so the two coherent beams of interference are with particular circular polarization. One of the incident beams, i.e. $\vec{E}_2$, is a wave propagating from a direction in the x-z plane making a small angle θ with respect to the z axis. The mathematical properties of two coherent beams are described as following:

$$\vec{E}_1(r, \phi, z) = E_0(r)e^{jm_1\phi}e^{-jkz}\,(\hat{x} - i\hat{y}) \tag{3-4}$$

$$\vec{E}_2(r, \phi, z) = E_0(r)e^{-jm_2\phi}\,e^{-jkz'}(\hat{x}' + i\hat{y}) \tag{3-5}$$

$$= E_0\,e^{-jm_2\phi}\,e^{-jkz\cos(\theta)}\,e^{-jkx\sin(\theta)}(\cos(\theta)\,\hat{x} - \sin(\theta)\hat{z} + i\hat{y}).$$

When the two waves are superposed, the field of their sum is

$$\vec{E}_{total}(r, \theta, z) = \hat{x}E_0[\,e^{jm_1\phi}e^{-jkz} + \cos(\theta)\,e^{-jm_2\phi}e^{-jkz\cos(\theta)}e^{-jkx\sin(\theta)}\,]$$

$$+ i\hat{y}E_0[-e^{jm_1\phi}e^{-jkz} + \cos(\theta)\,e^{-jm_2\phi}e^{-jkz\cos(\theta)}e^{-jkx\sin(\theta)}]$$

$$+ \hat{z}E_0\big[-\sin(\theta)\,e^{-jm_2\phi}e^{-jkz\cos(\theta)}e^{-jkx\sin(\theta)}\big].$$

The total field could be decomposed into three components depending on the state of polarization. The intensity profile as seen through a polarizer in the x-transmission axis can be described as following:

$$I_x(r, \phi, z) = \left|\vec{E}_{total\_x}\right|^2$$

$$= E_0{}^2\,[1 + \cos^2(\theta) + e^{j(m_1+m_2)\phi}e^{-jkz}\cos(\theta)\,e^{jkz\cos(\theta)}e^{jkx\sin(\theta)} +$$

$$e^{-j(m_1+m_2)\phi}\,e^{jkz}\cos(\theta)\,e^{-jkz\cos(\theta)}\,e^{-jkx\sin(\theta)}]. \tag{3-6}$$

Substituting $x = r\cos\phi$ into (3-6) due to consistency of the coordinate, we obtain

$$I_x = E_0{}^2\,[1 + \cos^2(\theta) + 2\cos(\theta)\cos\left((m_1 + m_2)\phi + kr\cos(\phi)\sin(\theta) + kz(\cos(\theta) - 1)\right)]$$

which can be abbreviated into

$$I_x \approx 1 + \cos\left((m_1 + m_2)\phi + kr\cos(\phi)\sin(\theta)\right) = 2\cos^2\left(\frac{m_1+m_2}{2}\phi + \frac{1}{2}kr\cos(\phi)\sin(\theta)\right).$$

In another case of using a polarizer with y transmission axis, the following formula
was derived :

$$I_y \approx 2\sin^2\left(\frac{m_1+m_2}{2}\phi + \frac{1}{2}kr\cos(\phi)\sin(\theta)\right). \tag{3-8}$$

When combining the Eqs. (3-7) and (3-8), the total field irradiance could be observed
by the CCD at exit of interferometer.

$$I = I_x + I_y \approx \cos^2\left(\frac{m_1+m_2}{2}\phi + \frac{1}{2}kr\cos(\phi)\sin(\theta)\right) + \sin^2\left(\frac{m_1+m_2}{2}\phi + \frac{1}{2}kr\cos(\phi)\sin(\theta)\right).$$

$$\tag{3-9}$$

In the experiment of synthesizing the cylindrical vector beams with titled angle,
the irradiance of emergent beam is I_x or I_y depending on the transmission axis of a
polarizer. The experiment result will be shown in the Chapter 3 where it is well match
with theoretical derivation.

3.2.1 Simulation of interference pattern

In this section we will discuss three cases which are distinguished with different
topological charge and tiled angle. For the case 1, $m_1=m_2=1$, it can be linked to our
synthesis of cylindrical vector beams and the interference pattern could be obtained
by experiment which is introduce in the chapter 3. From Eq. (3-9) the total irradiance
of interference can be can be abbreviated into

$$I = I_x + I_y \approx \cos^2\left(\phi + \frac{1}{2}kr\cos(\phi)\sin(\theta)\right) + \sin^2\left(\phi + \frac{1}{2}kr\cos(\phi)\sin(\theta)\right). \tag{3-10}$$

We can use mathematical software such as matlab to simulate intensity
distribution of the emergent beam by using the formula derived in previous
section. Fig. 3-2 (b - d) shows the interference pattern. If the tiled angle does not

equal to zero, the wires of the interference pattern become broader due to the decreasing tiled angle. The pattern of the first row is in the condition of x-transmission axis of polarizer. Similarly, the second row is in the condition of y-transmission axis of polarizer. We can find that they are spatially complementary between the first and second rows. From the relationship between pattern and tilted angle it can be applied to judge the precision of interferometer. As we decrease the titled angle carefully, the density of pipe wires decrease simultaneously. Till the tilted angle approaches zero, the fan-shaped pattern is observed as shown as Fig. 3-2 (a).

(a)   (b)   (c)   (d)
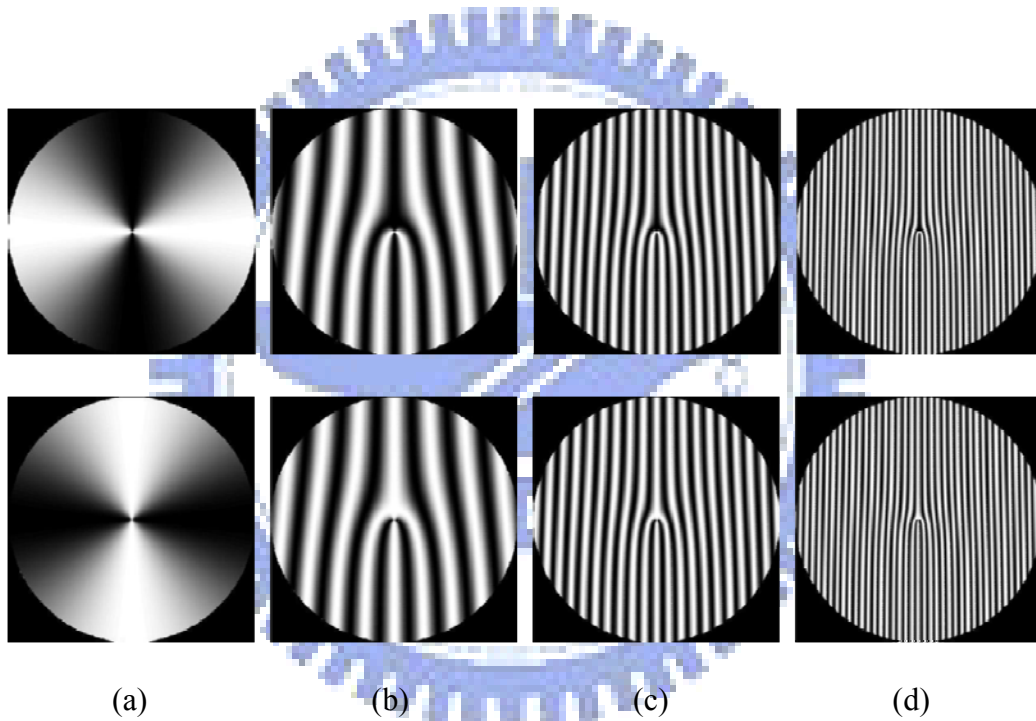
Fig. 3-2 Simulated interference pattern of $m = \pm 1$ in different angle (a) $0°$,(b) $0.02°$, (c) $0.05°$,(d) $0.1°$. The first row was represented in the x-transmission axis of polarizer. The second row was represented in the y-transmission axis of polarizer. Note that $m = m_1$ and $m = -m_2$. The density of pipe wires decrease when the titled angle is decreased.

For the case 2, $m_1 = m_2$, we consider that the beam with the same unsigned topological charge was interfered when the tilted angle is 0.02°. The formula which describes the intensity of emergent beam from the polarizer with x-transmission axis is

$$I \approx \cos^2\left(m_1\phi + \frac{1}{2}kr\cos(\phi)\sin(\theta)\right). \qquad (3\text{-}11)$$

Each of the interference patterns shown as Fig. 3-3 is with the same unsigned topological charge. The extra folk of interference pattern can be calculated by compare the wires of the upper plane of pattern with ones of the bottom plane. For instance, the m_{total} equal to 2 in the Fig. 3-3(a). In general, m_{total} can be expressed as

$$m_{total} = m_1 + m_2. \qquad (3\text{-}12)$$

According to this equation, we can know how many topological charges the emergent beam has by calculate the extra forks. Moreover, it is observed that all patterns have good symmetry in spatial 2D plane. This phenomenon of symmetry will be discussed in the case 3 in comparison with the different topological charge. Another observed phenomenon is that the interference of the odd topological charge leads to the dark wire of centerline in y-axis. In contrast, the interference of the even topological charge leads to the bright wire of midline in y-axis.

| (a) | (b) | (c) | (d) |
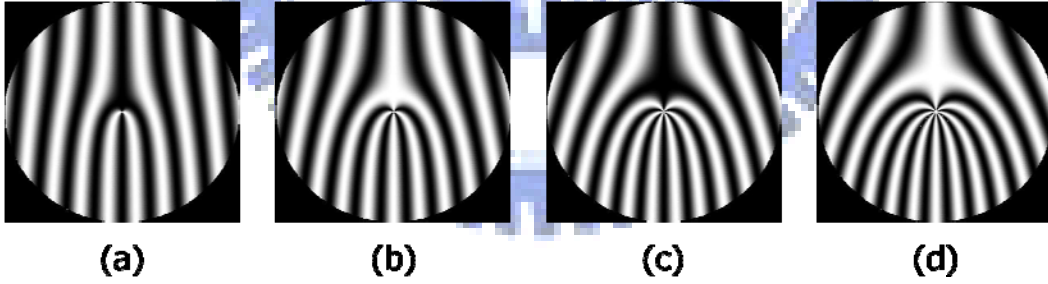
Fig. 3-3 Simulated interference pattern of spiral phase with $m =$ (a)±1, (b)±2, (c)±3, (d)±4. The tilted angle is 0.02° and the transmission axis of the polarizer is x-axis.

For the case 3, $m_1 \neq m_2$, the beam with the different unsigned topological charge was interfered when the tilted angle is 0.02°. The formula which describes the intensity of the emergent beam from the polarizer with x-transmission axis is

$$I \approx \cos^2\left(\frac{m_1+m_2}{2}\phi + \frac{1}{2}kr\cos(\phi)\sin(\theta)\right).$$

The interference pattern with different topological charge was shown as Fig. 3-4. The well symmetry of interference pattern in x axis is obtained due to the same unsigned topological charge, i.e. $m_1=m_2$. Interference of different unsigned topological charge leads to spatial asymmetry in x axis, as showed as Fig. 3-4(b)(d)(f)(h). The general rule to describe the symmetry of pattern is to check parity of the sum of topological charge. If the sum of m_1 and m_2 is even, the irradiance of good symmetry is observed. Differently, the odd number of summing m_1 and m_2 result in the spatial asymmetry in the bottom plane. Note that the general rule to judge the extra wires of pattern is the same with Eq. (3-12) derived in the case 2.

During the synthesis procedures as creating cylindrical vector beam, the precision of optical path of our setup can be checked by these interference patterns. Only the perfect supposition of two beams in the interferometer could lead to the perfect cylindrical vector beams. When one optical axis coincide with the other in the interferometer, we observe the fan shape pattern in the exit pupil plane due to the perfect overlap of high precision, as showed in the Fig. 3-5.
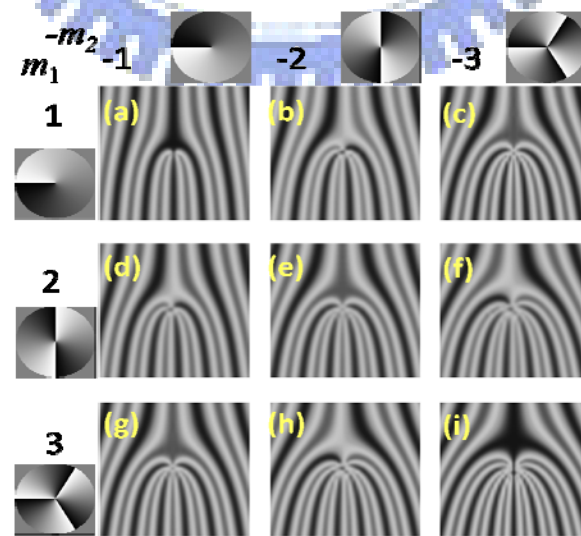
Fig. 3-4. Comparison of simulated interference pattern with different topological charge. The tilted angle is 0.02° and the transmission axis of the polarizer is x-axis.
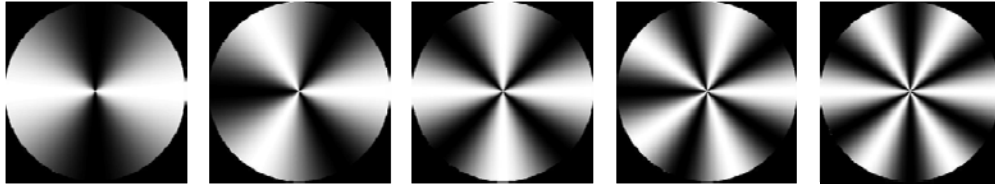
Fig. 3-5. Simulated patterns of superposition of $m_1 + m_2=$ (a) 2, (b) 3, (c) 4, (d) 5, (e)6 with no tilted angle.

3.3 Experiment

3.3.1 Synthesis of cylindrical vector beams

In this section we will show the experiment result of cylindrical vector beams. Based on the experiment setup discussed in previous section, the beam was combined with particular phase arrangement with specific circular polarization. First the correct phase arrangement was displayed in the SLM, and then the beam was reflected from SLM and was split into two beams by beamsplitter. In the interferometer each beam passed through a polarizer and a quarter wave plate and was transform from linear polarization to right handed or left handed circular polarization, as described in Fig. 2-2. The beam was superposed by the final beamsplitter and its irradiance was obtained from CCD.

A polarizer placed in front of CCD could be used to check the accuracy of state of polarization. Fig. 3-6 shows the irradiance of the synthesized beam with different transmission axis of a polarizer. In comparing the bright region of irradiance with the transmission axis of the polarizer, the derivation of angle between them can be adjusted. There are three methods to overcome the derivation due to the different length of the two arms of the interferometer. First, we can adjust the position of the

mirror or final beamsplitter to change the length of optical path. When the correct irradiance was obtained, the correct position of optical elements could be decided.

However, it is difficult to simultaneously adjust the element and keep the tilted angle which will lead to the change of irradiance. Another way is to change the phase arrangement on the SLM because the synthesis of cylindrical vector is based on the superposition of the opposite optical vortex. For instance, we control the rotation of the phase on the SLM to compensate the difference of optical paths of interferometer. Fig. 3-7 shows the respective rotation angle of particular phase on the SLM. We can adjust the angle φ until the correct irradiance is observed.

Finally, the inclined glass plate was put into one arm of interferometer to adjust the phase delay of interferometer. When inclined angle of glass plate is changing , we can find the best angle to correct the derivation.

| (a) | (b) | (c) |
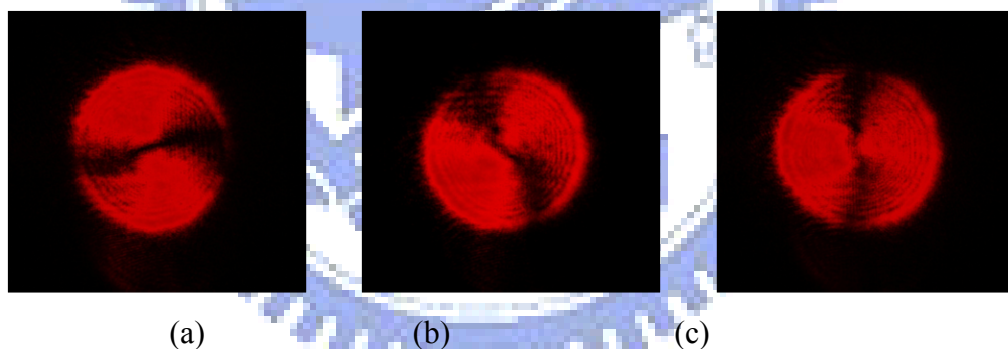
Fig. 3-6 The irradiance of the synthesized beam with different transmission axis of a polarizer. (a)0°, (b) 45°, (c) 90°.

(a)   (b)
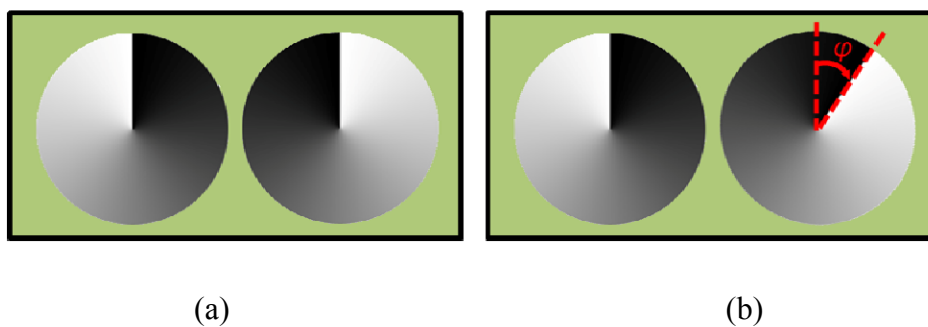
Fig. 3-7 The phase arrangement on the SLM. (a) Before adjustment. (b) After adjustment.

Cylindrical vector beams have special property in the focal region. The radially polarized beam have strong longitudinal polarization component which leads to generate extra small spot size at the focal point as simulated in Fig. 3-8(a). Furthermore, the azimuthally polarized beam will lead to spot of the donut-like shape due to the week longitudinal polarization component.

(a)   (b)
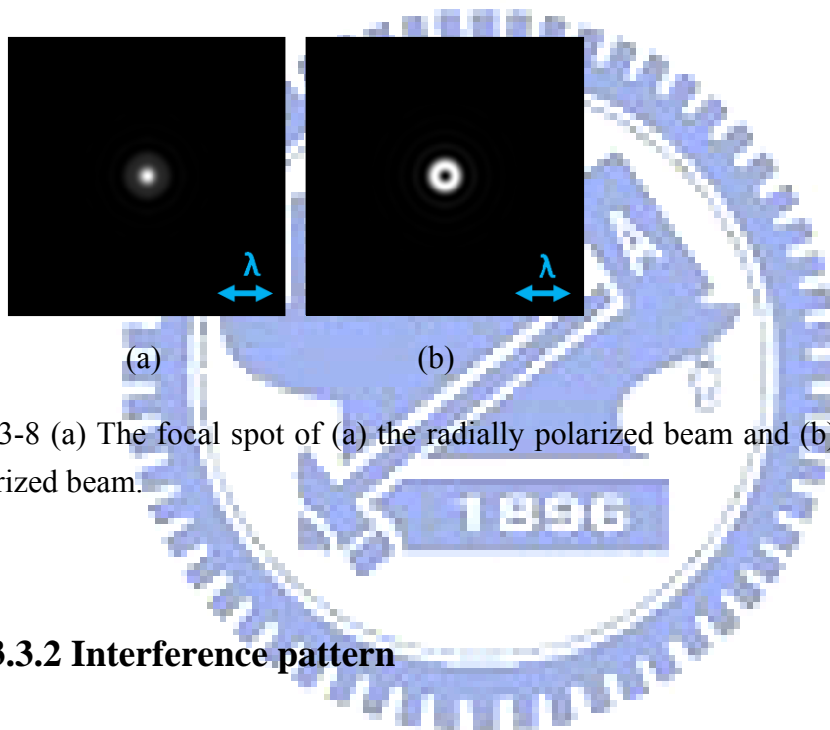
Fig. 3-8 (a) The focal spot of (a) the radially polarized beam and (b) the azimuthally polarized beam.

3.3.2 Interference pattern

The previous section mentions the synthesis of cylindrical vector beams with no tilted angle. If the two optical paths of interferometer don't coincide perfectly, the interference pattern was obtained by CCD. Therefore, we can adjust the tilted angle of mirror according to the patterns, as showed in Fig. 3-9. It's useful for us to do fine tuning. This experimental result is well matched with our simulation in Fig. 3-2.
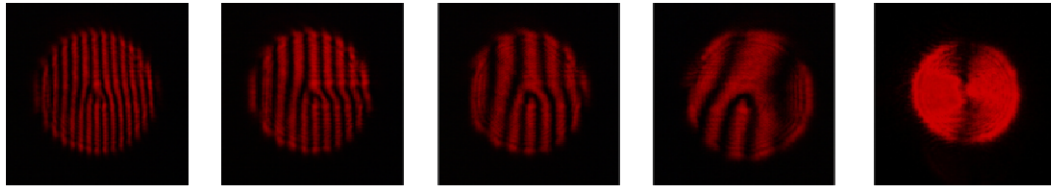
Fig. 3-9 Interference patterns with different tilted angle.

The optical phase is the dominate issue of producing the interference pattern which is easy to calculate the summation of unsigned topological charge. We can set the corresponding phase pattern on the SLM to obtain the interference pattern that we want. The results of the experiment were assembled in the table. From the table as the tilted angle is equal to zero, the wire shape of interference pattern was transformed to the fan shape.
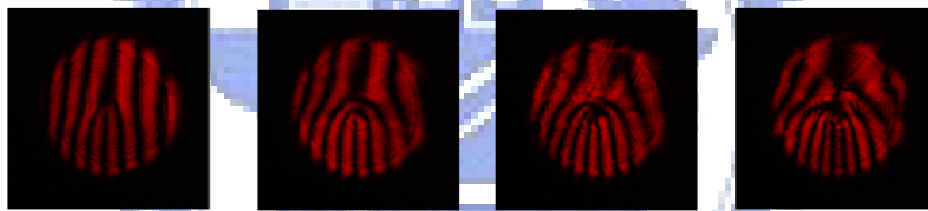
Fig. 3-10 Experimental interference pattern of spiral phase with m = (a)$\pm$1, (b)$\pm$2, (c)$\pm$3, (d)$\pm$4.
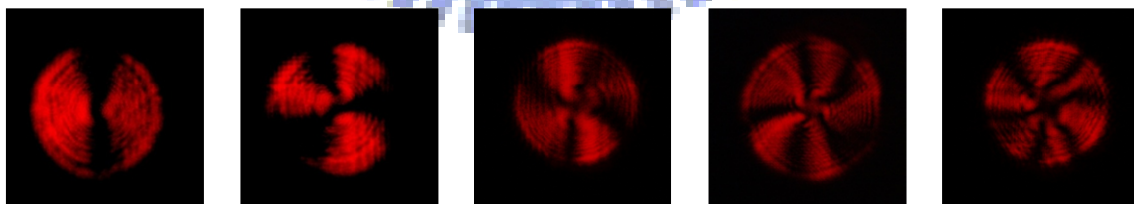
| (a) | (b) | (c) | (d) | (e) |

Fig. 3-11 Experimental interference patterns of superposition of $m_1 + m_2$= (a) 2, (b) 3, (c) 4, (d) 5, (e)6 with no tilted angle.

3.4 Summary

The experimental setup for synthesis process and interference has been completed by fine tuning. When the tilted angle approaches to $0°$ and the SLM provide the corresponding spiral phase, the fan shape intensity distribution depending on the transmission axis of a polarizer is most similar to the simulated one. By the results, the synthesis of cylindrical vector beam has been verified. Moreover, interference pattern of different topological charge shows the different extra wires and it's easy to check the number of topological charge.

Chapter 4

The spatially inhomogeneous polarized beam

The method was proposed to synthesize the inhomogeneous beam. Furthermore, the optimized setup has been utilized to enhance performance and reduce the diffraction effect. In order to verify this method, a demonstration based on the circular polarization approach will be completed.

4.1 Synthesis of 2-dimensional inhomogeneous polarized beams

Based on the interferometrical setup, an idea is proposed that arbitrary state of polarization can be obtained in spatial plane. The following sections include background information of mathematics and the analytical description of synthesis process. The first section focuses on the Jones calculus which is a useful tool to analyze the state of polarization.

4.1.1 Jones calculus

Jones Calculus which includes Jones matrix and Jones vector is a quantitatively mathematical description of polarized light. The operation of optical systems can be described by a cascade multiplication based on 2 x 2 matrices. Each component of the system has associated Jones matrix, and the analysis of the system as a whole is performed by multiplication of the 2 x 2 component matrices. Moreover, from the final vector of multiplication the state of polarization is clearly known at each stage of the calculation. The polarization information can be reduced to a vector, called the Jones vector. The field was described by the Jones vector whose vector components

are including Ex and Ey. From Eqs. $Ex = Ae^{j(-wt+kz)}$ and $Ey = Be^{j(-wt+kz+\Delta)}$, the Jones vector of the electric field is

$$\vec{E} = \begin{bmatrix} Ex \\ Ey \end{bmatrix} = e^{j(kz-wt)} \begin{bmatrix} A \\ Be^{j\Delta} \end{bmatrix}$$

where A and B are amplitude, and Δ is the phase retardation of the field. For convenience of calculation, the time-dependent term is omitted and then we denote the Jones vectors in their normalized forms. For instance, the linearly polarized beam $\begin{bmatrix} Ae^{j(kz-wt)} \\ 0 \end{bmatrix}$ can be normalized to $\begin{bmatrix} 1 \\ 0 \end{bmatrix}$.

When putting an optical component as a converter of the state of polarization from $[Ex \quad Ey]$ into $[E'x \quad E'y]$, the function of the optical component is represented by Jones matrix.

$$J' = \begin{bmatrix} E'x \\ E'y \end{bmatrix} = \begin{bmatrix} a & b \\ c & d \end{bmatrix} \begin{bmatrix} Ex \\ Ey \end{bmatrix} = MJ. \tag{4-1}$$

where J is the incident beam, J′ is the emergent beam, and M is the Jones matrix.

The Jones calculus also describes the optical functionality of components. This method is useful to describe the propagation of polarized light through optical elements such as polarizer and wave-plates. A polarizer is an optical element that passes a state of polarization by absorbing or reflecting the orthogonal mode of polarization. A wave-plate is an optical element that consists of an anisotropic material, which changes the phase of transmitted light depending on its polarization state. The following table summarizes the Jones vectors for common optical components.

Optical element	Jones matrix
Linear polarized with axis of transmission at angle ϕ	$\begin{bmatrix} \cos^2\phi & \cos\phi\sin\phi \\ \cos\phi\sin\phi & \sin^2\phi \end{bmatrix}$
Half-wave plate with fast axis in x-direction	$\begin{bmatrix} -i & 0 \\ 0 & i \end{bmatrix}$
Quarter-wave plate with fast axis in x-direction	$E^{i\pi/4} \begin{bmatrix} 1 & 0 \\ 0 & i \end{bmatrix}$
Quarter-wave plate with fast axis at angle 45°	$\frac{1}{\sqrt{2}} \begin{bmatrix} 1 & -j \\ -j & 1 \end{bmatrix}$
Quarter-wave plate with fast axis at angle -45°	$\frac{1}{\sqrt{2}} \begin{bmatrix} 1 & +j \\ +j & 1 \end{bmatrix}$

Table 4-1. The reference between optical element and Jones matrix.

Common optical elements are described by a 2×2 Jones matrix, enabling the description of the change of polarization states by multiplication of the Jones vector with the Jones matrix. Table 4-2 shows some examples of Jones vectors and Jones matrices of the optical elements.

Polarization	Jones vector	Illustration
Linear in x-direction	$\begin{bmatrix} 1 \\ 0 \end{bmatrix}$	
Linear in y-direction	$\begin{bmatrix} 0 \\ 1 \end{bmatrix}$	
Linear at 45°	$\begin{bmatrix} 1 \\ 1 \end{bmatrix}$	
Right circular	$\frac{1}{\sqrt{2}} \begin{bmatrix} 1 \\ -j \end{bmatrix}$	

Left circular	$\frac{1}{\sqrt{2}}\begin{bmatrix}1\\j\end{bmatrix}$	
Right elliptical	$\begin{bmatrix}A\\Be^{-j\Delta}\end{bmatrix}$	

Table 4-2 The reference between optical element and Jones vector.

4.1.2 Mathematics of synthesis

The synthesis of the inhomogeneous beams is based on the interferometrical circular approach. The key issue is to find the relationship between the phase retardation and polarization. Moreover, the derived formula can be used to modulate the spatial light modulator in our experiment. The associated instrument will be introduced in the chapter 3.

Consideration of letting the beam pass through the polarizer and a quarter wave plate can result in turning the x-polarized beam to left-handed circularly polarized beams. Jones matrix emergent from quarter-waveplate with fast axis at angle -45° is

$$\mathbf{E_L} = \frac{1}{\sqrt{2}}\begin{bmatrix}1 & +j\\+j & 1\end{bmatrix}\begin{bmatrix}Ex\\Ey\end{bmatrix} = \frac{1}{\sqrt{2}}\begin{bmatrix}1 & +j\\+j & 1\end{bmatrix}\begin{bmatrix}1\\0\end{bmatrix} = \frac{1}{\sqrt{2}}\begin{bmatrix}1\\j\end{bmatrix}.$$

Similarly, the x-polarized beam can be turned to right-handed circularly polarized beam. Jones matrix emergent from quarter-waveplate with fast axis at angle 45° is

$$\mathbf{E_R} = \frac{1}{\sqrt{2}}\begin{bmatrix}1 & -j\\-j & 1\end{bmatrix}\begin{bmatrix}1\\0\end{bmatrix} = \frac{1}{\sqrt{2}}\begin{bmatrix}1\\-j\end{bmatrix}.$$

The terms of phase retardation of light emergent from reflected SLM are $e^{-j\Delta}$ and $e^{j\Delta}$ respectively. As combining these beam, we can get the final vector which describes the state of polarization.

$$\mathbf{J}_l = \frac{1}{\sqrt{2}}\begin{bmatrix}1\\j\end{bmatrix}e^{-j\Delta} + \frac{1}{\sqrt{2}}\begin{bmatrix}1\\-j\end{bmatrix}e^{j\Delta} = \frac{1}{\sqrt{2}}\begin{bmatrix}e^{j\Delta} + e^{-j\Delta}\\j(e^{-j\Delta} - e^{j\Delta})\end{bmatrix} = \frac{2}{\sqrt{2}}\begin{bmatrix}\cos\Delta\\\sin\Delta\end{bmatrix} \qquad (4-2)$$

where J_l is Jones vector of the emergent beam at local point and the relative phase difference is the retardance Δ. Additionally, it is easy to control the state of polarization from SLM by referring to Eq. (4-2). When Δ is $0°$, the polarization is linear x-polarized beam. We put the retardance and Jones vector in order, as showed in Table 4-3. From this table, it is convenient for us to design the pattern on the SLM.

Retardance Δ	Jones vector	Illustration
0	$\begin{bmatrix} 1 \\ 0 \end{bmatrix}$	
$\frac{1}{4}\pi$	$\begin{bmatrix} 1 \\ 1 \end{bmatrix}$	
$\frac{1}{2}\pi$	$\begin{bmatrix} 0 \\ 1 \end{bmatrix}$	
$\frac{3}{4}\pi$	$\begin{bmatrix} -1 \\ 1 \end{bmatrix}$	
$\pi(-\pi)$	$\begin{bmatrix} -1 \\ 0 \end{bmatrix}$	
$-\frac{3}{4}\pi$	$\begin{bmatrix} -1 \\ -1 \end{bmatrix}$	
$-\frac{1}{2}\pi$	$\begin{bmatrix} 0 \\ -1 \end{bmatrix}$	
$-\frac{1}{4}\pi$	$\begin{bmatrix} 1 \\ -1 \end{bmatrix}$	

Table 4-3 The relationship of retardance and Jones vector.

In order to check feasibility of this method, we create a eight-zones polarization pupil to simulate the property of the inhomogeneous beams, as shown as showed in Fig. 4-1. Two cases of examples are radial-like and azimuthal-like beams. When taking radial-like polarization as an example, we can use the phase information with respective circular polarization as illustrated in Fig. 4-1 (b), (c). By using the software Diffract, we can simulate the propagation of radial-like beam passing

through the polarizer. Fig. 4-2 describes the simulation results depending on the transmission axis of polarizer. The result was brought into harmony with our prediction.

(a)   (b)   (c)   (d)   (e)   (f)
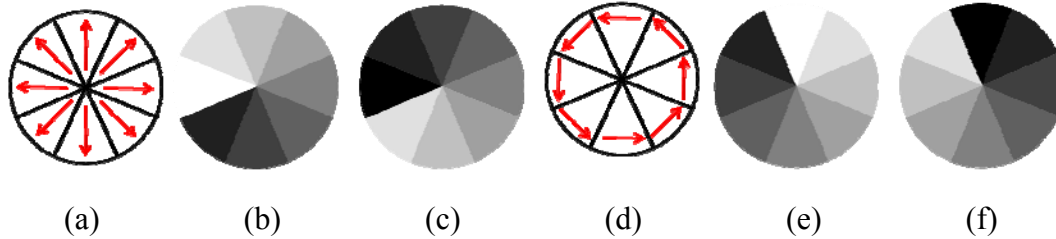
Fig. 4-1 Two examples of synthesizing the inhomogeneous beams. (a) Radial-like polarization with specific phase (b), (c) and (d) azimuthal-like beams polarization with specific phase (e), (f).

(a)   (b)   (c)   (d)
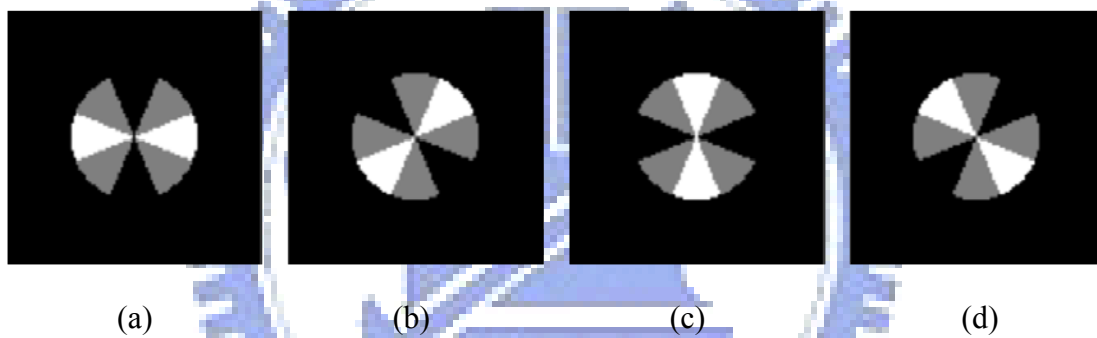
Fig. 4-2 The simulation of passing the radial-like beam through the transmission axis at the angle (a) $0°$, (b) $45°$, (c) $90°$, (d) $-45°$ of polarizer.

4.2 Synthesis of the inhomogeneous beams

In the demonstration, the SLM was utilized to generate localized phase information based on the relationship between retardance and polarization as mentioned in section 4.1.2. Therefore, in order to demonstrate correctly, it is important to make the optical paths of interference the same due to our derivation without any different path, so it needs more patients to adjust the position of beamsplitter or mirror. Another way of adjust the optical path is to put the glass plate

on the one arm of interferometer so the tilted angle of glass plate is used to compensate the difference of optical paths.

The following is the calibration procedure:

(1) The experimental setup gets ready and the corresponding phase pattern on the SLM can result in radially polarized beam.

(2) We can observe the irradiance of the emerge beam passing through the polarizer and adjust the tilted angle of two optical paths until the wire shape was transformed to the fan shape.

(3) If the angle of fan shape doesn't match with the angle of transmission axis of polarizer, we adjust the tilted angle of glass plate until they coincide.

(4) Finally we can put the pattern on SLM to synthesize the inhomogeneous beam we want.

Fig. 4-3 shows the experimental result of passing the radial-like beam through the transmission axis at the angle of polarizer.

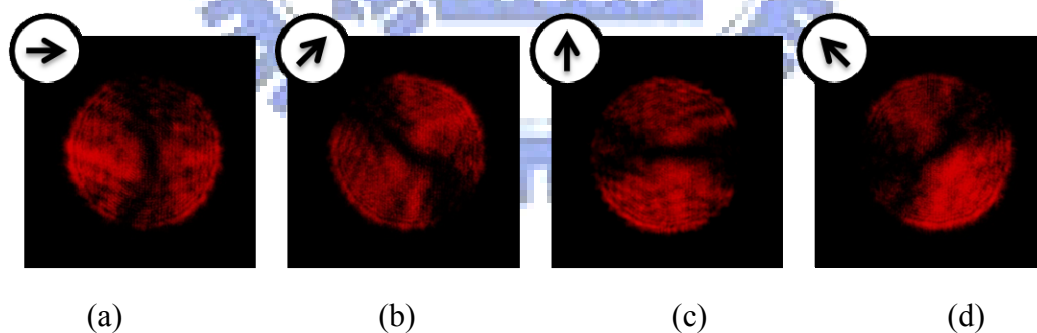| (a) | (b) | (c) | (d) |

Fig. 4-3 The experiment of passing the radial-like beam through a polarizer at the angle (a) 0°, (b) 45°, (c) 90°, (d) -45° of the transmission axis.

Another way to check the performance of the inhomogeneous beam is using the SNOM to observe the focal spot. The focal intensity distribution of the radial-like
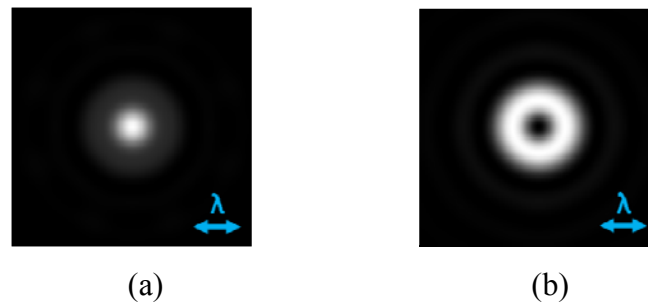
beam and azimuthal-like beam is shown in Fig. 4-4.

(a)   (b)

Fig. 4-4 The simulation of focusing (a)the radial-like beam and (b)azimuthal-like beam.

4.3 Optical encryption by polarization

In this section, we present an idea that the optical information can be carried by the beam and we can extract the information by using the polarizer, i.e. data encryption by polarization. Basically it is based on our circular approach of synthesizing the inhomogeneous beam. First, the information was edited by computer and stored to SLM, and then the beam was superposed by interferometer. At a receiver set, we can use the polarizer to choose the channel which is decided by the angle of transmission axis of a polarizer. Fig. 4-5 show output pattern by of a receiver with different transmission angle. We can see that the C-shape appear singly only in specific angle and disappeared in orthogonal angle. The choice of transmission axis leads to the particular pattern and the carried information can be extracted by the transmission control protocol at the receiver.

There are some issues to limit the development of this method. First, the uniformity of output pattern is not desirable, because it is easy to find the remaining intensity in dark region as showed in Fig. 4-5(a). If the variation of phase on SLM is

too large, the edge of the phase will result in the dark or bright line which spoiled the uniformity and caused the failure of reading the data. Finally, the optical component such as the diaphragm will lead to the airy disk due to diffraction effect ,and we will discuss more on the diffraction effect in next section.

(a)   (b)   (c)
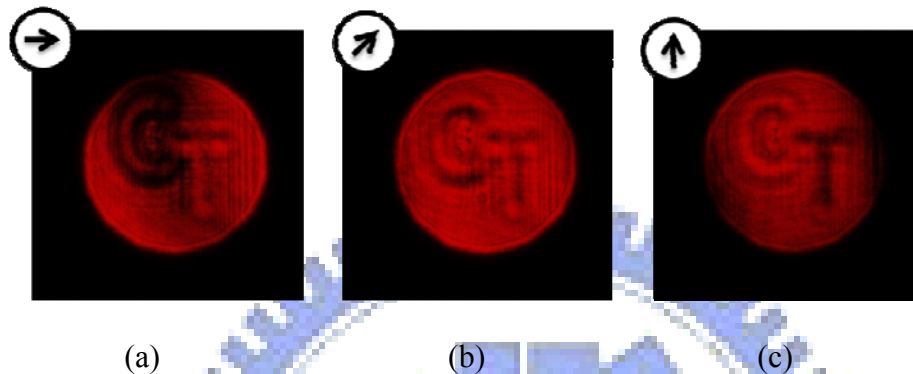
Fig. 4-5 The output of a receiver with different transmission angle. (a)$0°$, (b)$45°$, (c)$90°$.

4.4 Discussion of optimizing the performance

The performance of the emergent beam was diminished by the imperfect or physical property of the optical component which causes the aberration or diffraction effect.

4.4.1 The diffraction at boundaries

Diffraction can be understood by considering the wave nature of light. Huygen's principle states that each point on a propagating wavefront is an emitter of secondary wavelets. The combined focus of these expanding wavelets forms the propagating wave. Interference between the secondary wavelets gives rise to a fringe pattern that

rapidly decreases in intensity with increasing angle from the initial direction of propagation. Huygen's principle nicely describes diffraction, but rigorous explanation demands a detailed study of wave theory.

We consider the effects of that diffract screen introduced in the plane z = 0. Define the amplitude transmittance function of the aperture as the ratio of the transmitted field $U_t(x, y; 0)$ to the incident field amplitude $U_i(x, y; 0)$ at each (*x, y*) in the z = 0 plane [19],

$$t_A(x, y) = \frac{U_t(x,y;0)}{U_i(x,y;0)}. \tag{4-3}$$

Then the angular spectrum $A_i(\alpha/\lambda, \beta/\lambda)$ of the incident field and the angular spectrum $A_t(\alpha/\lambda, \beta/\lambda)$ of the transmitted field are related by the convolution theorem,

$$A_t\left(\frac{\alpha}{\lambda}, \frac{\beta}{\lambda}\right) = [A_i\left(\frac{\alpha}{\lambda}, \frac{\beta}{\lambda}\right) \otimes T\left(\frac{\alpha}{\lambda}, \frac{\beta}{\lambda}\right)] \tag{4-4}$$

where $T\left(\frac{\alpha}{\lambda}, \frac{\beta}{\lambda}\right) = \iint_{-\infty}^{\infty} t_A(x, y) \exp\left[-j2\pi(\frac{\alpha}{\lambda}x + \frac{\beta}{\lambda}y)\right] dxdy$, and $\otimes$ is the symbol for convolution. For example, if the incident plane-wave illuminates the diffracting structure normally, i.e.

$$A_i\left(\frac{\alpha}{\lambda}, \frac{\beta}{\lambda}\right) = \delta\left(\frac{\alpha}{\lambda}, \frac{\beta}{\lambda}\right), \tag{4-5}$$

and
$$A_t\left(\frac{\alpha}{\lambda}, \frac{\beta}{\lambda}\right) = \left[\delta\left(\frac{\alpha}{\lambda}, \frac{\beta}{\lambda}\right) \otimes T\left(\frac{\alpha}{\lambda}, \frac{\beta}{\lambda}\right)\right] = T\left(\frac{\alpha}{\lambda}, \frac{\beta}{\lambda}\right). \tag{4-6}$$

In this case, the transmitted angular spectrum is found directly by Fourier transforming the amplitude transmittance function of the aperture. Note that, if the diffracting structure is an aperture that limits the extent of the field distribution, this is a broadening of the angular spectrum of the disturbance, from smaller the aperture, the broader the angular spectrum behind the aperture.

In our experimental setup, the beam was cut by the diaphragm producing the dark rings. The diaphragm is the circular aperture so the transform of circle function is written

$$U(x,y,z) = \iint_{-\infty}^{\infty} A(fx,fy)circ\left(\sqrt{(\lambda f_x)^2 + (\lambda f_y)^2}\right)$$

$$\times \exp\left[j\frac{2\pi}{\lambda}\sqrt{1 - (\lambda f_x)^2 - (\lambda f_y)^2}z\right]\exp[-j2\pi(f_x x + f_y y)]\,dxdy. \quad (4\text{-}7)$$

where $f_x = \frac{\alpha}{\lambda}$ and $f_y = \frac{\beta}{\lambda}$, and the bandwidth limitation associated with evanescent waves was explicitly introduced through the use of a circ. function. Within the circular bandwidth, the modulus of the transfer function is unity but frequency-dependent phase shifts are introduced. The phase dispersion of the system is most significant at high spatial frequency as showed in Fig. 4-6 and vanishes as both f_x and f_y approach zero. In other words, the aperture is the smaller, and the angular spectrum behind the aperture is the broader. For any fixed spatial frequency pair the phase dispersion increases as the distance of propagation z increases.
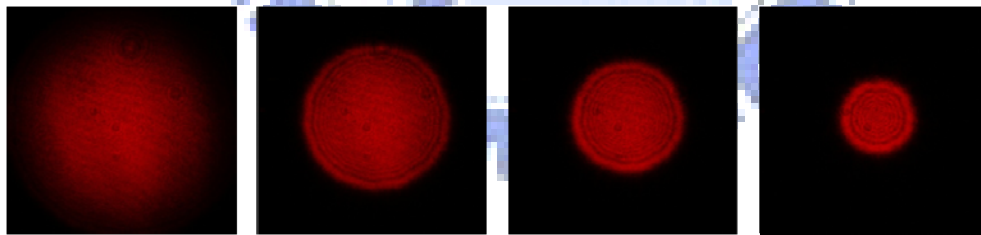

Fig. 4-6 The diffraction at boundaries

Based on the previous discussion our experimental setup could be redesigned as depicted as Fig. 4-7. The diaphragm was moved behind the final beamsplitter due to increasing of phase dispersion as the distance of propagation z increases. Nevertheless, the diffraction remains because the beam was cut by the boundaries of diaphragm, so

we add spatial filter to diminish the dark rings.
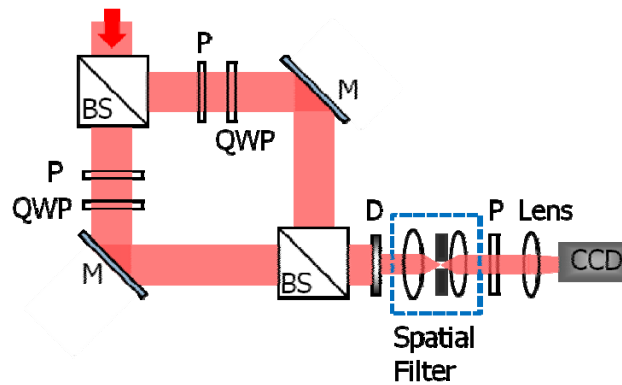
Fig. 4-7 The schematic of optimized setup. BS: beamsplitters, M: mirror, and

D: diaphragm.

4.5 Summary

In closing we presented and demonstrated the idea of the synthesis of inhomogeneous beam and the data encryption by polarization which allows us to conveniently edit the arbitrary local phase delay by SLM. In addition, some of their obvious limit have been found and been diminished by adding the spatial filter and reset the position of diaphragm.

Chapter 5   *Con*

clusions and Future work

5.1 Conclusions

In this thesis, we demonstrated a circularly polarization interference method to generate the spatially inhomogeneous polarized beams which include cylindrical vector beams and the 8-zone radial-like and azmuthal-like polarized beams. Based on the numerical and experimental studies, different polarization states can be switched by loading different phase arrangement subject to the SLM. The focal irradiance of cylindrical vector beams is nearly equal to the size of their vector diffraction limited spot size.

From a set of systematic studies, we found that the interference patterns can be used to not only make a distinction between radially and azimuthally polarized beams but also ensure the experimental precision. And from interference patterns caused by optical vortex, the topological charges lead to the extra pipe-line patterns and fan-shaped pattern. As the tilted angle of two optical paths approaches to zero, the density of pipe line will decrease and yield a fan-shaped pattern. Moreover, we redesigned the experimental setup in order to diminish the diffraction at the boundary and improve the performance of emergent beam.

The flexibility of SLM yields an opportunity to synthesize arbitrary inhomogeneous polarization for other application. The present work unambiguously demonstrates the beam could locally have different states of polarization in 2D plane, and it will trigger future studies addressing near field fabrication with a resolution

beyond the diffraction limit of light as well as fundamental studies and theories of photo-induced nano movements in polymers.

5.2 Future Work

The uniformity of output irradiance and the purity of polarization is the big issue of our experiment. In our thesis we have tried to improve the performance of our synthesized beams. Moreover it is not good enough so these beams should be improved by advanced method.

The paper presents a fast and accurate method for the surface correction of spatial light modulators [20]. The method uses one single image of a focused doughnut beam, created by the SLM, to find the corresponding phase hologram with the Gerchberg Saxton (GS) algorithm. They have demonstrated, both experimentally and in computer simulations, that the GS algorithm is able to reconstruct hardware phase errors on the order of one or two wavelengths. The presented method promises applicability in research areas where the light phase has to be modified by flexible devices like SLMs or micro mirror arrays with high accuracy. The method could also be used to optimize the entire optical setup, since the determined correction function also corrects distortions which are introduced by other optical elements.

In closing, we will combine the phase correction and our experimental setup to improve the uniformity and the purity of output irradiance and develop the desired spatially inhomogeneous polarized beam for other application.

Reference

[1] S. Quabis, R. Dorn, M. Eberler, O. Glo¨ckl, G. Leuchs, "Focusing light to a tighter spo," *Opt. Commun.* **179**, 1–7 (2000).

[2] E. A. Saleh, M. C. TEICH, *Fundamental of Photonics*, (1991).

[3]E. Wolf, *Progress in Optics*, pp. 296-317 (1999).

[4] M.W. Beijersbergen, L. Allen, H.E.L.O. van der Veen, and J.P. Woerdman, "Astigmatic laser mode converters and transfer of orbital angular momentum," *Opt. Comm.* **96**, 123-132 (1996).

[5] L. Allen, M.W. Beijersbergen, R.J.C. Spreeuw, and J.P. Woerdman, "Orbital angular momentum and the transformation of Laguerre-Gaussian modes," *Phys. Rev. A* **45**, 8185-8189 (1992).

[6] A. V. Nesterov, V. G. Niziev, and V. P. Yakunin, "Generation of high-power radially polarized beam," *J. Phys. D Appl. Phys.* **32**, 2871-2875 (1999).

[7] G. Machavariani, Y. Lumer, I. Moshe, A. Meir, and S. Jackel, " Efficient extracavity generation of radially an azimuthally polarized beams" *Opt. Lett.* **32**, No. 11, 1468-1470 (2007).

[8] A. A. Tovar, "Production and propagation of cylindrically polarized Laguerre Gaussian laser beams," *J. Opt. Soc. Am. A*, **15**, 27052711 (1998).

[9] Z. Bomzon, G. Biener, V. Kleiner, and E. Hasman, "Radially and azimuthally polarized beams generated by space-variant dielectric subwavelength gratings," *Opt. Lett.* **27**, 285-287 (2002).

[10] B. Jia, X. Gan, and Min Gu, "Direct measurement of a radially polarized focused evanescent field facilitated by a single LCD", *Opt. Express* **13**, No18, September (2005)

[11] S. C. Tidwell, D. H. Ford, and W. D. Kimura, "Generating radially polarized beams interferometrically," *Appl. Opt.* **29**, 2234-2239 (1990).

[12] R. Oron, S. Blit, N. Davidson, and A. A. Friesem, etc, "The formation of laser beams with pure azimuhtal or radial polarization," *Appl. Phys. Lett.* 77, pp. 3322-3324 (2000).

[13] MErd´elyi and Zs Bor, "Radial and azimuthal polarizers," *J. Opt. A: Pure Appl. Opt.* **8** 737–742 (2006).

[14] Tidwell S. C., Ford D. H. and Kimura W. D., "Transporting and focusing radially polarized laser beams," *Opt. Eng.* **31** 1527–31(1992).

[15] D. P. Biss and T. G. Brown, "Cylindrical vector beam focusing through a dielectric interface," *Opt. Express* **9**, No. 10, 490-497 (2001).

[16] Q. Zhan, "Trapping metallic Rayleigh particles with radial polarization," *Opt. Express* **12**, 3377 (2004).

[17] S. C. Tidwell, G. H. Kim, and W. D. Kimura, "Efficient radially polarized laser beam generation with a double interferometer," *Appl. Opt.* 32, 5222-5229 (1993).

[18] Lars Egil Helseth, "Roles of polarization, phase and amplitude in solid immersion lens systems," *Opt. Commun.* **191**, 161-172 (2001).

[19] Joseph. W. Goodman , *Introduction to Fourier Optics*, 3rd edition.

[20] A. Jesacher, A. Schwaighofer, S. F¨urhapter, C. Maurer, S. Bernet, and M. Ritsch-Marte, "Wavefront correction of spatial light modulators using an optical vortex image,*" Opt. Express* **15**, 5801-5808 (2007).